

Evaporation of black holes in flat space entangled with an auxiliary universe

Akihiro Miyata,^a Tomonori Ugajin^{b,c}

^a*Institute of Physics, University of Tokyo, Komaba,
Meguro-ku, Tokyo 153-8902, Japan*

^b*Center for Gravitational Physics, Yukawa Institute for Theoretical Physics, Kyoto University, Kitashirakawa Oiwakecho, Sakyo-ku, Kyoto 606-8502, Japan*

^c*The Hakubi Center for Advanced Research, Kyoto University, Yoshida Ushinomiyacho, Sakyo-ku, Kyoto 606-8501, Japan*

E-mail: miyata@hep1.c.u-tokyo.ac.jp,
tomonori.ugajin@yukawa.kyoto-u.ac.jp

ABSTRACT: We study a thermofield double type entangled state on two disjoint universes A and B , where one of the universes is asymptotically flat containing a black hole. As we increase the entanglement temperature, this black hole receives back-reaction from the stress energy tensor of the state. This results in lengthening of the wormhole region in the black hole interior, and decreasing of its horizon area, both of which are key features of an evaporating black hole. We then compute the entanglement entropy on the universe A through the island formula, and argue that it naturally follows the Page curve of an evaporating black hole in flat space. We also study the effects of local operations in the gravitating universe with the black hole. We find that they accelerate the evaporation of the black hole, therefore disrupt the entanglement between two universes. Furthermore, we observe that depending on whether the operation can be regarded as an LOCC or not, the behavior of the entanglement entropy changes. In particular, when the operation is made neither in the entanglement wedge of the radiation system or that of the black hole, the transition between the island phase and the no-island phase can happen multiple times.

Contents

1	Introduction	1
2	Setup	4
2.1	Two disjoint asymptotically flat universes	4
2.2	Islands in the setup	5
2.3	Embedding of two universes	6
3	An asymptotically flat black hole and its radiation entropy	6
3.1	Penrose diagrams	8
3.2	Quantum extremal surface	11
4	Black hole interior in the presence of shock wave	12
4.1	Dilaton part	14
4.2	Classical extremal surfaces	14
4.3	CFT entropy part	16
4.3.1	CFT entropy for a single interval	17
4.3.2	CFT entropy for two disjoint intervals	19
4.4	Quantum extremal surfaces	19
4.5	QESs with non-trivial CFT entropy	23
4.6	The entanglement entropy	28
5	Conclusion	29
A	Entanglement entropy and local quench for two disjoint intervals	30

1 Introduction

Recently it has been claimed that in the presence of semi-classical gravity, the island formula gives a correct prescription to compute entanglement entropy [1–5]. This formula is inspired by the holographic entanglement entropy formula [6–8] and its quantum corrections [9, 10] in the AdS/CFT correspondence. When this formula is applied to a semi-classical black hole which is evaporating due to Hawking radiation, the entropy of the radiation naturally follows the Page curve [11, 12]. This provides a resolution of the black hole information loss problem,

and implies that semi-classical gravity is consistent with unitarity of quantum theory. The way this new rule provides the correct entropy involves a region called “island” in the black hole. This island region naturally arises, when we compute the entanglement entropy using a gravitational path integral through the replica trick [4, 5]. In fact, the rule to evaluate a gravitational path in the semi-classical limit appears to include all saddles consistent with given boundary conditions. It was argued that there is an overlooked gravitational saddle in the Hawking’s calculation of the radiation entropy. This new saddle is called a replica wormhole, and this saddle gives the dominant contribution after the Page time. See for a review of this topic [13].

One way to efficiently study black hole evaporation is, introducing another auxiliary universe, say universe A which we assume to be non-gravitating, and consider an entangled state $|\Psi\rangle_{AB}$ on A and the original gravitating universe B with the black hole¹. One can think of this new system being generated out of the system in the single universe with an evaporating black hole, by gathering all Hawking quanta, and sending them to the auxiliary universe. Therefore the entanglement of the $|\Psi\rangle_{AB}$ mimics the one of the Hartle-Hawking state on the evaporating black hole. This setup has been used to study the entropy of Hawking radiation of two dimensional black holes in anti-de Sitter (AdS) space and de Sitter in JT gravity [28, 29]. See for studies with a similar approach [4, 30]. Other applications of the island formula to de Sitter space can be found in [21, 30–32] Indeed the entanglement entropy of this new system on AB naturally follows a Page curve as a function of the entanglement temperature.

In this paper, we generalize this analysis to black holes in flat space. Evaporation of such two dimensional asymptotically flat black holes, as well as time evolution of their radiation entropy have been studied since early 90’s [33–35]. Previous applications of the island formula to black holes in asymptotically flat space can be found, for example in [36–43]. Since the total state $|\Psi\rangle_{AB}$ induces the stress energy tensor expectation value $\langle\Psi|T_{ab}|\Psi\rangle$ to the gravitating universe, the black hole in this universe receives back-reaction from it. As in the cases of dS and AdS black holes in JT gravity, we show that this back-reaction is crucial to get the Page curve for the black hole in flat space. Two key effects of the back-reaction on the black hole are the following. First, it makes the wormhole in the interior region longer, second it reduces the horizon area. This implies, when we compute the entanglement entropy $S(\rho_A)$ of the non-gravitating universe using the island formula, it starts to decrease when the entanglement temperature is increased above some threshold value. This is in contrast to the case of AdS black holes, where the entropy is saturating to some constant value. The decrease of the

¹Another way to efficiently study the evaporation process is to holographically realize the system, by introducing branes on which gravitational degrees of freedom are living [1, 4, 14–27].

entropy is plausible, because a black hole in flat space evaporates through Hawking radiation, and loses its entropy.

We believe our setup clarifies several ambiguities in the previous discussions on the island formula applied to asymptotically flat black holes. In the previous discussions, the radiation subsystem (the heat bath) is often naively taken to be the region R located far away from the black hole, but it is still gravitating. However, such a choice for the radiation region R is worrisome because of several reasons. First, there is no consistent way to define a “region” in the presence of gravity, in a diffeomorphism invariant manner. In addition, the Hilbert space of quantum gravity never factorizes into the Hilbert space on R and its complement, due to the edge modes on the boundary of the region R . Second, when the heat bath is gravitating, the naive island formula is no longer valid, as has been shown in the recent papers [19, 23, 44, 45]. This is because in the setup there is a novel wormhole connecting the gravitating bath and the black hole appears in the path integral for the Rényi entropies. This is a concrete realization of the ER = EPR [46] slogan, which predicts the existence of such a wormhole connecting the early radiation and the black hole interior.

These two concerns are avoided in a very clear manner in our setup of two disjoint universes. Namely, in our setup since the radiation region is located on the non-gravitating universe A which differs from the gravitating universe with the black hole, there is no ambiguity in defining the radiation region from the first place. This in particular means that our definition of the entanglement entropy is unambiguous. Also in our setup, since two universes are disjoint we can safely turn off gravity in one of the universes, thus we do not need to worry about the existence of the wormhole connecting the bath and the black hole.

We then addressed the question of whether the entropy computed from the island formula is operationally meaningful from the quantum information theoretic point of view. To this end we study perturbations of the black hole by local operations in the gravitating universe. One way to model such a local operation is applying an operator well localized in the region of the interest, and this protocol is known as a local quench. Time evolution of the entanglement entropy in such quench processes have been extensively studied, for example in [47–57]. We find such local operations “accelerate” the evaporation, especially when the operators are inserted in the interior of the black hole. Effects of such shock waves on the radiation entropy has been studied in [2, 58–62] using the island formula.

We indeed find that our results obtained from the island formula are operationally meaningful. For instance when the insertion is made either in the entanglement wedge of the radiation or in the similar wedge of the black hole, then the resulting entanglement entropies always decreases. This is consistent with the interpretation that such a local operator inser-

tion is an LOCC (local operations and classical communications.)

This paper is organized as follows. In section 2 we explain our setup, and the previous results on the island formula in this setup in detail. In section 3, we introduce the black hole solution of our interest, and study how it is deformed due to the back-reaction of the stress energy tensor expectation value of the total state. We then use the island formula to compute the entanglement entropy of the non-gravitating universe A. The result naturally follows a Page curve of an evaporating black hole. In section 4, we study the Page curve in the presence of local operations in the gravitating universe. After classifying possible quantum extremal surfaces, we discuss effects of the local operations to the entanglement entropy. We conclude this paper in section 5. Appendix A we review and discuss time dependence of the entanglement entropy in a local quench in a two dimensional conformal field theory with a large central charge.

2 Setup

2.1 Two disjoint asymptotically flat universes

Let us first explain the setup we consider in this paper. First of all, we prepare two disjoint universes, say A and B which are asymptotically flat (see figure 1). We then define two identical CFTs, on each universe A and B . For simplicity, in this paper, we only consider two dimensional spacetimes. Furthermore, we turn on semi-classical gravity on the universe B . Thus the effective action of each universe reads

$$\log Z_A = \log Z_{\text{CFT}}, \quad \log Z_B = -I_{\text{grav}} + \log Z_{\text{CFT}}. \quad (2.1)$$

As the gravitational part I_{grav} of the above effective action, we choose the CGHS action [33],

$$I_{\text{grav}} = \frac{1}{4\pi} \int dx^2 \sqrt{-g} (\Phi R - \Lambda), \quad (2.2)$$

which is a theory of gravity in two dimensional asymptotically flat space. This action involves two fields, namely dilaton Φ and metric $g_{\mu\nu}$. Also, we introduced an auxiliary parameter Λ , for the later purpose².

The total Hilbert space of this system is naturally bipartite $H_A \otimes H_B$. Since these two universes A and B are disjoint, they can not exchange classical information, but states on A and B can be entangled quantum mechanically. In this paper, we are interested in the

²The reader should not confuse this parameter Λ with a cosmological constant.

structure of the entanglement of the states on the bipartite Hilbert space. To study this concretely, on the bipartite system we will consider the thermofield double (TFD) state

$$|\Psi\rangle = \sum_{i=0}^{\infty} \sqrt{p_i} |i\rangle_A |\psi_i\rangle_B, \quad p_i = \frac{e^{-\beta E_i}}{Z(\beta)}, \quad (2.3)$$

where $Z(\beta)$ is a normalization factor which makes sure the condition $\langle\Psi|\Psi\rangle = 1$, $|i\rangle_A$ is an energy eigenstate of the CFT on the non-gravitating universe A, and $|\psi_i\rangle_B$ is the same energy eigenstate on the gravitating universe B. Although they are identical states, since gravity is acting on the universe B, and properties of the state is affected by this, so we instead write them differently. β in (2.3) characterizes the amount of the entanglement in this state. For this reason, $1/\beta$ is sometimes called the entanglement temperature.

2.2 Islands in the setup

In our previous papers [28, 29], we studied the entanglement entropy $S(\rho_A)$ of the TFD state (2.3) on the non-gravitating universe A. This quantity is defined by the von Neumann entropy

$$S(\rho_A) = -\text{tr} \rho_A \log \rho_A, \quad \rho_A = \text{tr}_B |\Psi\rangle\langle\Psi| \quad . \quad (2.4)$$

This von Neumann entropy is computed by the replica trick, ie first compute the Rényi entropy $\text{tr} \rho_A^n$, which has a path integral representation on the gravitating universe B, then at the end of the calculation send $n \rightarrow 1$. This gravitational path integral is evaluated in the semi-classical limit $G_N \rightarrow 0$, by including all saddles consistent with given boundary conditions. In particular, by taking into account a wormhole which connects all replicas (replica wormhole), we obtained the following formula for the entanglement entropy,

$$S(\rho_A) = \min\{S_{\text{no-island}}, S_{\text{island}}\}. \quad (2.5)$$

$S_{\text{no-island}}$ in the above formula coincides with the CFT thermal entropy $S_{\text{no-island}} = S_\beta(B)$,

$$S_{\text{th}}(B) = - \sum_i p_i \log p_i, \quad (2.6)$$

with p_i defined in (2.3). The other contribution S_{island} in the above formula is given by taking the extremum of the generalized entropy,

$$S_{\text{island}} = \text{Ext}_{\bar{C}} [\Phi(\partial\bar{C}) + S_\beta[\bar{C}] - S_{\text{vac}}[\bar{C}]] \equiv \text{Ext}_{\bar{C}} S_{\text{gen}}[\bar{C}] \quad (2.7)$$

over all possible intervals \bar{C} in the gravitating universe B. $\Phi(\partial\bar{C})$ is the “area term” of the generalized entropy, which is in the current case given by the sum of the dilaton values at

the boundary of the interval \bar{C} . Also, $S_\beta[\bar{C}]$ is the entanglement entropy of thermal states on \bar{C} , and $S_{\text{vac}}[\bar{C}]$ is the entropy of the vacuum state. Since the TFD state is pure on the total system AB, the generalized entropy satisfies $S_{\text{gen}}[\bar{C}] = S_{\text{gen}}[AC]$. This implies the interval C in the gravitating universe B can be identified with the island in our setup.

We are interested in the behavior of the entanglement entropy $S(\rho_A)$ as we tune the entanglement temperature $1/\beta$, especially when the gravitating universe B contains a black hole. It was argued that [28, 29], in the low temperature regime $\beta \gg 1$, since $S_{\text{no-island}} < S_{\text{island}}$ this entanglement entropy (2.5) coincides with the thermal entropy $S_{\text{th}}(B)$, which is an analogue of the Hawking's result for the radiation entropy of evaporating black holes. Also, this implies the entropy is linearly growing, as we increase the entanglement temperature $1/\beta$. At sufficiently high temperature $S_{\text{no-island}}$ is larger than S_{island} . According to the formula (2.5), in this regime the entanglement entropy is given by S_{island} , instead of the naive Hawking's entropy $S_{\text{no-island}}$. Furthermore, in this limit, S_{island} almost coincides with the entropy of the black hole in the gravitating universe B. This is how the Page curve of an evaporating black hole is reproduced in the current setup.

2.3 Embedding of two universes

One way to study the setup is to embed the system to a larger Minkowski space M , as in figure 1. Each universe is a wedge in the larger space. The non-gravitating universe is the left wedge of M and similarly the gravitating universe is the right wedge. To be more specific, let us define the light-cone coordinates $x^\pm = x \pm t$ on each universe. Also, let (w^+, w^-) be coordinates of the larger Minkowski space M . The embedding map is defined by

$$w^\pm = e^{\frac{2\pi}{\beta}} x^\pm. \quad (2.8)$$

The non-gravitating universe A is mapped to the left wedge of M , $w^\pm < 0$ and the gravitating universe B is mapped to the right wedge of M , $w^\pm > 0$. Also the thermofield double state on AB is mapped to the global Minkowski vacuum of M .

3 An asymptotically flat black hole and its radiation entropy

The purpose of this paper is to study a similar entropy in asymptotically flat spacetime, using the island formula (2.5). To do so, we need to specify the dilaton profile Φ which appears in the generalized entropy (2.7). Since the thermofield double state induces the thermal stress

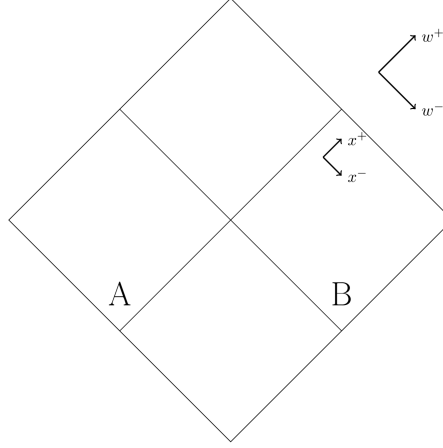


Figure 1: We consider a system with two disjoint asymptotically Minkowski spaces, A and B. In this figure, these universes are embedded in a larger Minkowski space.

energy tensor expectation value $\langle \Psi | T_{\pm\pm} | \Psi \rangle$ on the gravitating universe B , this dilaton receives back-reaction from it.

In the CGHS model with the action (2.2), the metric is always fixed to the flat one, as the variation of the action with respect to Φ sets $R = 0$. We will find it convenient to use the compact coordinates (x^+, x^-) , in which the flat metric is given by

$$ds^2 = -\frac{dx^+ dx^-}{\cos^2 x^+ \cos^2 x^-}, \quad -\frac{\pi}{2} \leq x^\pm \leq \frac{\pi}{2}. \quad (3.1)$$

These coordinates are related to the standard coordinates (X^+, X^-) with the metric $ds^2 = -dX^+ dX^-$, by $X^\pm = \tan x^\pm$. In the coordinate system, $x^+ = \pm \frac{\pi}{2}$ and $x^- = \pm \frac{\pi}{2}$ correspond to asymptotic infinities of the spacetime.

The equations of motion for the dilaton is given by

$$\nabla_a \nabla_b \Phi - g_{ab} \nabla^2 \Phi = \frac{\Lambda}{2} g_{ab} - 2\pi \langle \Psi | T_{ab} | \Psi \rangle. \quad (3.2)$$

In general, in the light-cone gauge where the metric takes the form,

$$ds^2 = -e^{2\omega} dx^+ dx^-, \quad (3.3)$$

these equations of motion are reduced to

$$-e^{2\omega} \partial_\pm [e^{-2\omega} \partial_\pm] \Phi = 2\pi \langle \Psi | T_{\pm\pm} | \Psi \rangle, \quad \partial_+ \partial_- \Phi = 2\pi \langle \Psi | T_{+-} | \Psi \rangle + \frac{\Lambda}{4} e^{2\omega}. \quad (3.4)$$

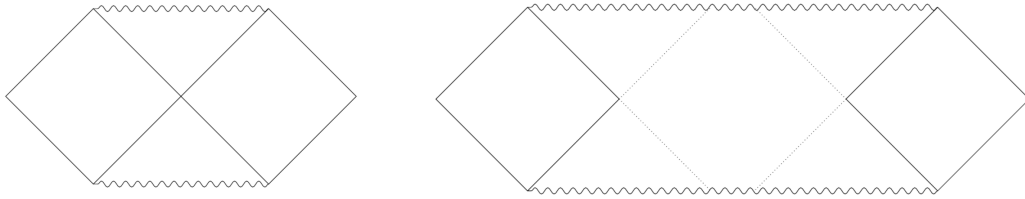


Figure 2: **Left:** The Penrose diagram of the black hole without the back-reaction. **Right:** The Penrose diagram of the black hole with the back-reaction of the source (3.6). It develops a long wormhole region in its interior.

The Sourceless solution

Let us first discuss the dilaton profile when the stress energy tensor is vanishing $\langle \Psi | T_{ab} | \Psi \rangle = 0$. In our setup, this happens when the entanglement temperature is low, $\beta \rightarrow \infty$. It reads

$$\Phi_0 = \phi_0 + \frac{\Lambda}{4} \tan x^+ \tan x^-, \quad (3.5)$$

where Λ is the parameter in the CGHS action (2.2). As we will see, this dilaton profile corresponds to an asymptotically flat eternal black hole, whose Penrose diagram is identical to the standard 4d Schwarzschild eternal black hole (refer to the left panel of Fig. 2).

The Solution with the source

As we increase the entanglement temperature, it is no longer possible to neglect the back-reaction of the stress energy tensor to the dilaton profile. The stress energy tensor expectation value of the thermofield double state (2.3) is,

$$\langle \Psi | T_{\pm\pm} | \Psi \rangle = \frac{c}{24\pi} \left(\frac{2\pi}{\beta} \right)^2. \quad (3.6)$$

By solving the equations (3.4) for Φ , we get

$$\Phi_\beta = \phi_0 + \frac{\Lambda}{4} \tan x^+ \tan x^- - X_\beta (x^+ \tan x^+ + x^- \tan x^-), \quad X_\beta \equiv \frac{c}{24} \left(\frac{2\pi}{\beta} \right)^2. \quad (3.7)$$

This solution corresponds to an eternal black hole with a long interior region (the right panel of Fig. 2).

3.1 Penrose diagrams

Now having presented the dilaton profile of our interest (3.7), let us discuss the causal structure of the spacetime described by the profile. Since it turns out that it corresponds to an

eternal black hole, we are interested in the location of the singularity and the event horizon. A useful fact is that, the dilaton is vanishing $\Phi = 0$ at the black hole singularity. Also, the bifurcation surface of the black hole is a critical point $\partial_{\pm}\Phi = 0$. The entropy of the black hole is given by the dilaton value at the critical point.

The sourceless solution

As a warm-up, let us describe the causal structure of the dilaton profile (3.5) without the source. In this case, the location of the singularity satisfies

$$\Phi_0 = 0 \leftrightarrow \tan x^+ \tan x^- = -\frac{4\phi_0}{\Lambda}. \quad (3.8)$$

In the standard coordinates (X^+, X^-) , this singularity is just a hyperbola $X^+X^- = -4\phi_0/\Lambda$, which is expected. This singularity intersects with the right future null infinity $x^+ = \frac{\pi}{2}$ at $x^- = 0$. Similarly, it intersects with the left future infinity $x^- = -\frac{\pi}{2}$ at $x^+ = 0$. This fixes the location of the event horizon to $x^+ = 0$ and $x^- = 0$. Indeed, this black hole has only one bifurcation surface, ie, at $x^{\pm} = 0$. The value of the dilaton at the bifurcation surface is $\Phi(0) = \phi_0$, which is equal to the entropy of the black hole, and is independent of Λ .

The solution with the source

The structure of the spacetime is eventually deformed by turning on the stress energy tensor (3.6), due to the back-reaction, which is described by the dilaton profile Φ_{β} (3.7). We can read off the location of the singularity in the deformed spacetime from Φ_{β} . Near the right future null infinity $x^+ = \frac{\pi}{2}$, the dilaton profile is approximated as

$$\Phi_{\beta} = \frac{\Lambda}{4} \tan x^+ \left(\tan x^- - \frac{2\pi X_{\beta}}{\Lambda} \right), \quad x^+ \rightarrow \frac{\pi}{2}. \quad (3.9)$$

Therefore, the singularity intersects with the future infinity at $x^- = x_c^-$ with,

$$\tan x_c^- = \frac{2\pi X_{\beta}}{\Lambda}. \quad (3.10)$$

As we increase the entanglement temperature $\beta \rightarrow 0$, X_{β} in the right hand side gets large, and the intersection approaches spatial infinity, $x_c^- \rightarrow \frac{\pi}{2}$ with $x^+ = \frac{\pi}{2}$. Similarly, the singularity intersects with the left future null infinity $x^- = -\frac{\pi}{2}$ at $x^+ = x_c^+$ with

$$\tan x_c^+ = -\frac{2\pi X_{\beta}}{\Lambda}, \quad (3.11)$$

again in the high temperature limit, it satisfies $x_c^+ \rightarrow -\frac{\pi}{2}$, so this intersection approaches the opposite spatial infinity. Since the dilaton profile (3.7) is invariant under time reflection $x^+ \leftrightarrow x^-$, the singularity intersects with the past null infinity in a similar fashion. Namely it intersects with the right past null infinity $x^- = \frac{\pi}{2}$ at $x^+ = -x_c^+$ with (3.11) and the left past null infinity $x^+ = -\frac{\pi}{2}$ at $x^- = -x_c^-$ with (3.10). In summary, as one increases the entanglement temperature, the singularity of the black hole comes closed to the reflection symmetric slice $x^+ = x^-$.

This also fixes the location of the event horizon of the black hole. The right future horizon of the black hole is at $x^- = x_c^-$ with (3.10). Similarly the left future horizon is at $x^+ = -x_c^+$. Since these two future horizons do not intersect on the reflection symmetric slice $x^+ = x^-$, this black hole contains a region in its interior, which is causally inaccessible from asymptotic infinities (the right panel of figure 2). Such a region is called a causal shadow region. The fact that the black hole singularity approaches the reflection symmetric slice as we increase the entanglement temperature means the causal shadow region gets larger and larger in this limit.

One can also confirm this by finding locations of the bifurcation surfaces (x_H^+, x_H^-) which satisfy $\partial_\pm \Phi_\beta = 0$. Because of the symmetry $x^+ \leftrightarrow x^-$ of the dilaton profile (3.7), these bifurcation surfaces satisfy $x_H^+ = x_H^- \equiv y$, and

$$\frac{\Lambda}{4} \tan y - X_\beta (\cos y \sin y + y) = 0. \quad (3.12)$$

We are interested in the $\beta \rightarrow 0$ limit, where the two solutions $y = y_\pm$ of the equation the equation (3.12) satisfy

$$\tan y_\pm = \frac{4X_\beta y_\pm}{\Lambda}. \quad (3.13)$$

Both of these bifurcation surfaces get close to the spatial infinity, $y_\pm \rightarrow \pm \frac{\pi}{2}$. The dilaton value at these bifurcation surfaces in the same limit is given by

$$\Phi_\beta(x_H^\pm) = \phi_0 - \frac{(\pi X_\beta)^2}{\Lambda}. \quad (3.14)$$

Notice that the dilaton value $\Phi_\beta(x_H^\pm)$ at the horizon decreases as we increase $1/\beta$. This means that, as we increase the entanglement between the two universes $\beta \rightarrow 0$, the back-reaction of the CFT stress energy tensor makes the horizon area of the black hole smaller. This is closely related to fact that quantum mechanically, a black hole in flat space evaporates by emitting of Hawking quanta. Indeed our setup can be regarded as an idealization of the black hole plus a radiation system. The radiation degrees of freedom is modeled by the CFT

degrees of freedom in our setup, and the entanglement of the CFT thermofield double state between A and B is the avatar of the entanglement in the Hartle-Hawking state. Therefore the increase of the entanglement of the TFD state (which we do by hand), captures the late time physics of the actual black hole evaporation process, and as a result, the black hole in our setup loses its entropy.

We can not have a semi-classical description of the black hole, at the very final stage of the evaporation. This is because, as we increase the entanglement temperature, both future and past singularities come close to the reflection symmetric slice, and eventually touch the slice. This critical temperature can also be read off from the dilaton values at the bifurcation surfaces (3.14), where it becomes zero.

3.2 Quantum extremal surface

Now, let us compute the entanglement entropy $S(\rho_A)$ of the universe A through the island formula (2.5) with (2.7). For this purpose we need to extremize the generalized entropy for all possible intervals \bar{C} whose end points are identified with quantum extremal surfaces. In the calculation, it is reasonable to assume that \bar{C} is on the reflection symmetric slice $x^+ = x^-$, and is given by the union of two intervals $\bar{C} = \bar{C}_1 \cup \bar{C}_2$, $\bar{C}_1 : -\frac{\pi}{2} < x^+ \leq -\frac{\pi x}{2}$, $\bar{C}_2 : \frac{\pi x}{2} \leq x^+ < \frac{\pi}{2}$ with $0 < x < 1$. The generalized entropy reduces to a function of single variable x ,

$$S_{\text{gen}}(x) = 2\Phi_\beta(x) + \frac{2c}{3} \log \left[\frac{\beta}{\pi \varepsilon_{\text{UV}}} \sinh \frac{\pi^2}{2\beta} (1-x) \right] - \frac{2c}{3} \log \left[\frac{1}{\varepsilon_{\text{UV}}} \sin \frac{\pi}{2} (1-x) \right], \quad (3.15)$$

where ε_{UV} is the UV cutoff. We give a plot of the above function in the left panel of figure 4.

In the $\beta \rightarrow 0$ limit, the quantum extremal surfaces almost coincide with the classical bifurcation surfaces of the black hole. This is because the QESs approach the spatial infinity and therefore the CFT entropy part in $S_{\text{gen}}(x)$ is vanishing in this limit. As a result, the island is identified with the causal shadow region in the black hole interior (figure 3).

By combining these results, we get the following approximate expression for the entanglement entropy $S(\rho_A)$,

$$S(\rho_A) = \begin{cases} S_{\text{no-island}} = \frac{\pi^2 c}{3\beta} & \beta > \beta_c \\ S_{\text{island}} = 2 \left[\phi_0 - \frac{(\pi X_\beta)^2}{\Lambda} \right] & \beta < \beta_c, \end{cases} \quad (3.16)$$

where β_c is the critical inverse temperature satisfying $S_{\text{no-island}} = S_{\text{island}}$. We plot the Page curve by using the above expression in the right panel of figure 4.

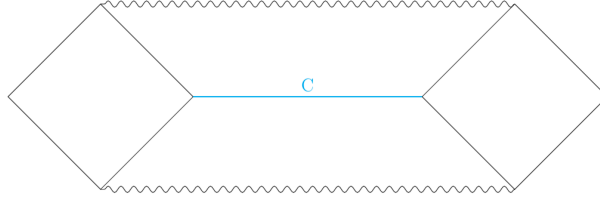


Figure 3: The location of the island C in the black hole with the back-reaction, denoted by the blue line.

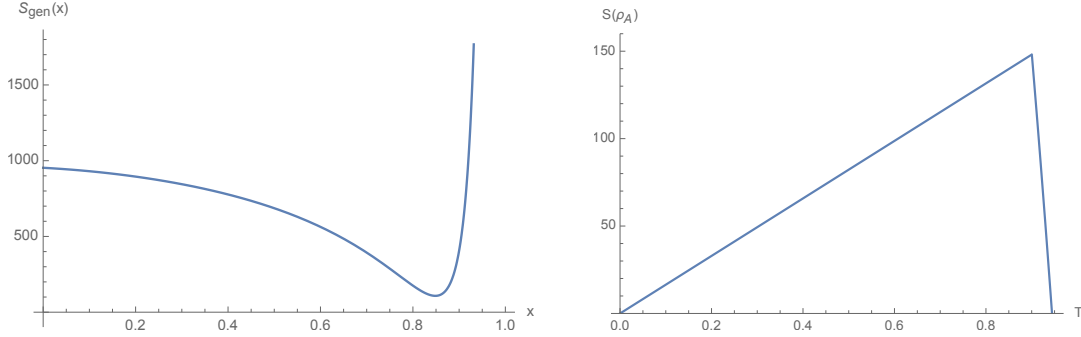


Figure 4: **Left** :Plot of the generalized entropy $S_{\text{gen}}(x)$ as a function of the size of the island in the interior. **Right**: The resulting Page curve as a function of the entanglement temperature $T = 1/\beta$. Here we set the parameters to be $\phi_0 = 1700$, $\Lambda = 500$, $c = 50$ in both figures and $\beta = 1$ for left figure.

4 Black hole interior in the presence of shock wave

We have seen, by making the entanglement between two universes stronger, the size of the black hole interior in the gravitating universe B gets larger. So in some sense this interior region is created by the entanglement between the degrees of freedom in the gravitating universe B and the ones in the other (non-gravitating) universe. To sharpen the intuition, in this section, we would like to ask how do the local operations in the gravitating universe B change the entanglement.

We imagine an experimental physicist in a lab has this system AB of two disjoint universes (or the larger Minkowski space containing AB as in figure 1), and can perform any local operation on the gravitating universe B even in the black hole interior. Such local operation can be modeled by a shock wave in the null directions along which the CFT stress energy tensor has a delta functional peak. Such a peak of the stress energy tensor can back-react to the dilaton profile through the equations of motion (3.4).

We start from the state $|\Psi\rangle$ on AB , prepared by inserting a local operator \mathcal{O}_B in the

gravitating universe B to the thermofield double state

$$|\Psi\rangle = (1_A \otimes \mathcal{O}_B) |TFD\rangle = \frac{1}{\sqrt{Z(\beta)}} \sum_{i=0}^{\infty} e^{-\frac{\beta}{2} E_i} |i\rangle_A \otimes \mathcal{O}_B |\psi_i\rangle_B. \quad (4.1)$$

We are interested in its entanglement entropy $S(\rho_A)$ of the above state, which is computed by the island formula (2.5). Since $S_{\text{no-island}}$ does not change by the insertion of \mathcal{O}_B , we focus on S_{island} given by the generalized entropy,

$$S_{\text{gen}} = \text{Ext}_{\bar{C}} [\Phi(\partial\bar{C}) + S_{\beta,E}[\bar{C}] - S_{\text{vac}}[\bar{C}]], \quad (4.2)$$

where $S_{\beta,E}[\bar{C}]$ denotes the CFT entanglement entropy in the presence of the shock wave created by \mathcal{O}_B .

Let (x_0^+, x_0^-) be the location of the insertion of the operator \mathcal{O} . Then the reduced density matrix of the universe B is

$$\rho = \text{tr}_A |\Psi\rangle\langle\Psi| = \frac{1}{Z_{\mathcal{O}}} e^{-\varepsilon H} \mathcal{O}(x_0^+, x_0^-) \rho_{\beta} \mathcal{O}^\dagger(x_0^+, x_0^-) e^{-\varepsilon H}. \quad (4.3)$$

Here we introduced a UV regulator ε , to make the density matrix normalizable, and the normalization factor

$$Z_{\mathcal{O}} = \langle \mathcal{O}(2i\varepsilon) \mathcal{O}(0) \rangle_{\beta}, \quad (4.4)$$

which ensures $\text{tr } \rho = 1$. We also denote, $\langle \cdots \rangle_{\beta} \equiv \text{tr}[\rho_{\beta} \cdots]$.

This local operator \mathcal{O} affects the stress energy tensor expectation value, and therefore the dilaton profile. The stress energy tensor expectation value can be computed by the three point functions $\text{tr}[\rho_{\beta} T_{\pm\pm} \mathcal{O} \mathcal{O}]$, and it reads

$$\langle \Psi | T_{++}(x^+) | \Psi \rangle = \frac{c}{24\pi} \left(\frac{2\pi}{\beta} \right)^2 + E_{\text{Shock}} \delta(x^+ - x_0^+), \quad \langle \Psi | T_{--}(x^-) | \Psi \rangle = \frac{c}{24\pi} \left(\frac{2\pi}{\beta} \right)^2 + E_{\text{Shock}} \delta(x^- - x_0^-), \quad (4.5)$$

in the $\varepsilon \rightarrow 0$ limit. The coefficient of the delta functions is related to the conformal dimension Δ of this local operator

$$E_{\text{Shock}} = \frac{\Delta}{\varepsilon}. \quad (4.6)$$

Therefore, the insertion of a local operator creates a pair of shock waves in the black hole geometry, one is left moving and the other is right moving. The existence of these shocks is manifested by the delta functional peaks of the CFT stress energy tensor expectation value. For simplicity, we write $E \equiv E_{\text{Shock}}$ below.

4.1 Dilaton part

Let us discuss in detail how the shock wave changes the dilaton Φ . It satisfies the following equations of motion,

$$\begin{aligned} -e^{2\omega} \partial_{\pm} (e^{-2\omega} \partial_{\pm} \Phi) &= 2X_{\beta} + E \delta(x^{\pm} - x_0^{\pm}), \\ \partial_+ \partial_- \Phi &= \frac{\Lambda}{4} e^{2\omega}. \end{aligned} \quad (4.7)$$

These equations are obtained by substituting the stress tensor expectation value (4.5) to (3.4) for arbitrary $\langle T_{\pm\pm} \rangle$. By solving these equations, we obtain, the dilaton profile in the presence of shock wave,

$$\begin{aligned} \Phi &= \phi_0 + \frac{\Lambda}{4} \tan x^+ \tan x^- - X_{\beta} (x^+ \tan x^+ + x^- \tan x^-) \\ &\quad - E \cos^2 x_0^+ (\tan x^+ - \tan x_0^+) \theta(x^+ - x_0^+) - E \cos^2 x_0^- (\tan x^- - \tan x_0^-) \theta(x^- - x_0^-), \end{aligned} \quad (4.8)$$

where $\theta(x)$ is the step function,

$$\theta(x) = \begin{cases} 1 & x > 0 \\ 0 & x < 0. \end{cases} \quad (4.9)$$

4.2 Classical extremal surfaces

Now we would like to specify the classical extremal surfaces in the spacetime with the dilaton profile (4.8). We will see that the actual locations of these surfaces highly depend on where we insert the local operator. In the right wedge of the local operator $x^{\pm} > x_0^{\pm}$, the dilaton coincides with $\Phi_{\beta,E}$ defined by

$$\begin{aligned} \Phi_{\beta,E} &= \phi_0 + \frac{\Lambda}{4} \tan x^+ \tan x^- - X_{\beta} (x^+ \tan x^+ + x^- \tan x^-) \\ &\quad - E \cos^2 x_0^+ (\tan x^+ - \tan x_0^+) - E \cos^2 x_0^- (\tan x^- - \tan x_0^-). \end{aligned} \quad (4.10)$$

In the left wedge $x^{\pm} < x_0^{\pm}$, it agrees with the original profile $\Phi = \Phi_{\beta,E=0} \equiv \Phi_{\beta}$ (3.7), see figure 5. We also argued that in the absence of the shock wave, ie, $E = 0$, the black hole has a causal shadow region in its interior, so it has two bifurcation surfaces. In the presence of the shock, the dilaton profile (4.8) has also two critical points, one is near the left spatial infinity $(x^+, x^-) = (-\frac{\pi}{2}, -\frac{\pi}{2})$ and the other is near the right spatial infinity $(x^+, x^-) = (\frac{\pi}{2}, \frac{\pi}{2})$. In this section, we only consider the operator insertions, which do not change the location of the left horizon of the undeformed dilaton Φ_{β} . This is equivalent to restrict the range of the insertion to $0 < x_0^+ + x_0^-$. Under this restriction, we can focus on the change of the location

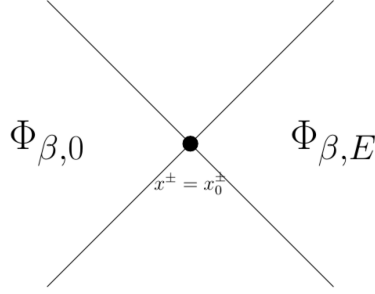


Figure 5: The dilaton profile (4.8) in the presence of the shock wave. In the right wedge of the local operator, $x^\pm > x_0^\pm$, we have $\Phi = \Phi_{\beta,E}$ with (4.10). On the left wedge, $x^\pm < x_0^\pm$, the dilaton profile coincides with $\Phi_{\beta,0}$, which is identical to (3.7) .

of the right critical point below. The discussion for operator insertions in the $x_0^+ + x_0^- < 0$ region can be made similarly.

To identify the right extremal surface, it is convenient to introduce two characteristic points of the dilaton profile Φ . First, let $x^\pm = x_H^\pm(0)$ be the critical point of the original dilaton profile $\Phi_\beta(x^\pm)$, ie

$$\partial_\pm \Phi_\beta|_{x^\pm = x_H^\pm(0)} = 0 \rightarrow \tan x_H^\pm(0) = \frac{2\pi}{\Lambda} X_\beta. \quad (4.11)$$

The second characteristic point is $x^\pm = x_H^\pm(E)$, which is the critical point of the deformed dilaton profile $\Phi_{\beta,E}$ (4.10). It satisfies

$$\tan x_H^\pm(E) = \frac{4}{\Lambda} \left(\frac{\pi}{2} X_\beta + E \cos^2 x_0 \right). \quad (4.12)$$

These are candidates of the extremal surfaces of the total dilaton (4.8), but whether these are the critical points of the actual dilaton (4.8) depends on the location of the local operator $x^\pm = x_0^\pm$.

In order to simplify the discussion below, instead of exhausting all possible cases, let us first consider the symmetric insertions $x_0^+ = x_0^- \equiv x_0$. Now these two candidate extremal surfaces are also symmetric, ie they are on the reflection symmetric slice : $x_H^+(0) = x_H^-(0) \equiv x_H(0)$, and $x_H^+(E) = x_H^-(E) \equiv x_H(E)$. In general, the relation $x_H(0) < x_H(E)$ holds. In this setup, there are three distinct cases for the operator insertions (see figure 5). Namely, the location of the operator is (1) behind the original horizon $x_0 < x_H(0)$, (2) in the middle of two horizons, $x_H(0) < x_0 < x_H(E)$ and (3) in the exterior of the deformed horizon $x_H(E) < x_0$.



Figure 6: Three possible locations of the local operator \mathcal{O} on the reflection symmetric slice $\Sigma : x^+ = x^-$. **Left :** When $x_0 < x_H(0) < x_H(E)$, the extremal surface is at $x^\pm = x_H(E)$. **Middle :** When $x_H(0) < x_0 < x_H(E)$, both $x^\pm = x_H(0)$ and $x^\pm = x_H(E)$ are extremal. **Right:** When $x_H(0) < x_H(E) < x_0$, the extremal surface is at $x^\pm = x_H(0)$.

Case 1

In the first case, the local operator \mathcal{O} is inserted to the left of the original horizon : $x_0 < x_H(0)$ (left panel of figure 6). In this case, only the extremal surface is the deformed horizon $x^\pm = x_H(E)$. This is because $x^\pm = x_H(0)$ is not a critical point of the dilaton profile (4.8), since around this point, this profile coincides with the deformed one $\Phi_{\beta,E}$ (4.10), due to the condition $x_0 < x_H(0)$. The dilaton value at the extremal surface is given by $\Phi(x_H(E)) = \Phi_{\beta,E}(x_H(E))$.

Case 2

In the second case, the local operator is inserted in between two would be extremal surfaces $x_H(0) < x_0 < x_H(E)$ (middle panel of figure 6). In this case, both horizons $x^\pm = x_H^\pm(0)$ and $x^\pm = x_H^\pm(E)$ are actually extremal surfaces of the dilaton profile (4.8).

Case 3

In the third case, the local operator is inserted to the right of the deformed horizon $x_H(E) < x_0$ (right panel of figure 6). In this case, only the extremal surface is the original horizon $x^\pm = x_H^\pm(0)$. This is again because the deformed horizon $x^\pm = x_H^\pm(E)$ is not the critical point of the dilaton. The dilaton value at the extremal surface is given by $\Phi_\beta(x_H^\pm(0))$.

4.3 CFT entropy part

The second ingredient of the generalized entropy (4.2) is the CFT entropy $S_{\beta,E}[\bar{C}]$ of the density matrix (4.3) on \bar{C} in the gravitating universe B . Because we focus on the high temperature limit $\beta \rightarrow 0$, this region is the disjoint union of two pieces $\bar{C} = \bar{C}_1 \cup \bar{C}_2$, as in the previous section. We put the coordinates of \bar{C} as follows;

$$\begin{cases} x_2^\pm = -\frac{\pi}{2}, \\ x_3^\pm = x_3 \pm t_3, \end{cases} \quad \text{for } \bar{C}_1$$

$$\begin{cases} x_5^\pm = x_5 \pm t_5, & \text{for } \bar{C}_2 \\ x_6^\pm = \frac{\pi}{2}. \end{cases}$$

In the $\beta \rightarrow 0$ limit, $x_3^\pm \rightarrow x_2^\pm$ and $x_5^\pm \rightarrow x_6^\pm$ holds. Therefore, in the absence of the shock wave $E = 0$, the CFT entanglement entropy for $\bar{C} = \bar{C}_1 \cup \bar{C}_2$ at finite temperature β is given by

$$\begin{aligned} S_\beta[\bar{C}] = & \frac{c}{6} \log \left[\frac{\beta}{\pi \varepsilon_{UV}} \sinh \left(\frac{\pi}{\beta} (x_3^+ - x_2^+) \right) \right] + \frac{c}{6} \log \left[\frac{\beta}{\pi \varepsilon_{UV}} \sinh \left(\frac{\pi}{\beta} (x_3^- - x_2^-) \right) \right] \\ & + \frac{c}{6} \log \left[\frac{\beta}{\pi \varepsilon_{UV}} \sinh \left(\frac{\pi}{\beta} (x_6^+ - x_5^+) \right) \right] + \frac{c}{6} \log \left[\frac{\beta}{\pi \varepsilon_{UV}} \sinh \left(\frac{\pi}{\beta} (x_6^- - x_5^-) \right) \right]. \end{aligned} \quad (4.13)$$

We also need the CFT entropy for $\bar{C} = \bar{C}_1 \cup \bar{C}_2$ at zero temperature, and it is given by

$$\begin{aligned} S_{\text{vac}}[\bar{C}] = & \frac{c}{6} \log \left[\frac{1}{\varepsilon_{UV}} \sin (x_3^+ - x_2^+) \right] + \frac{c}{6} \log \left[\frac{1}{\varepsilon_{UV}} \sin (x_3^- - x_2^-) \right] \\ & + \frac{c}{6} \log \left[\frac{1}{\varepsilon_{UV}} \sin (x_6^+ - x_5^+) \right] + \frac{c}{6} \log \left[\frac{1}{\varepsilon_{UV}} \sin (x_6^- - x_5^-) \right]. \end{aligned} \quad (4.14)$$

4.3.1 CFT entropy for a single interval

Next, we discuss the entanglement entropy $S_{\beta,E}[\bar{C}]$ in the presence of a shock wave. This kind of entanglement entropy was studied in [51], which we review in Appendix A. As a warm-up, let us compute the entanglement entropy $S_{\beta,E}[\bar{C}]$ of the single interval,

$$\bar{C} : x_5^\pm < x^\pm < x_6^\pm = \frac{\pi}{2}. \quad (4.15)$$

which ends at the asymptotic infinity $x_6^\pm = \frac{\pi}{2}$. In presenting the expression of the CFT entropy, it is convenient to first fix the subsystem \bar{C} ie, fixing x_5^\pm .

This entanglement entropy can be computed, first writing the Rènyi entropy $\text{tr} \rho_{\bar{C}}^n$ by a four point function involving twist operators,

$$\text{tr} \rho_{\bar{C}}^n = \text{tr} \left[\rho_\beta \mathcal{O}^{\otimes n}(x_1) \sigma_n(x_5) \sigma_{-n}(x_6) \mathcal{O}^{\otimes n}(x_4) \right], \quad (4.16)$$

and taking $n \rightarrow 1$ limit of the correlator. Here x_1 and x_4 are related to x_0 through (A.4). When the central charge of the theory is large $c \gg 1$, and its spectrum is sparse, the right hand side can be approximated by the vacuum conformal block with a choice of branch [51]. Again details can be found in the Appendix.

The possible form of the CFT entropy is constrained by the causal relation between the location of the operator $x^\pm = x_0^\pm$ and the region \bar{C} [47–57, 63]. Indeed, the insertion creates shock waves, both left moving and right moving, which is roughly speaking interpreted as

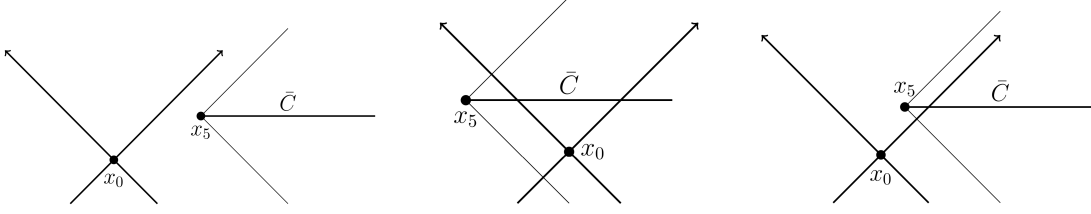


Figure 7: Three possible causal relations between the operator at $x^\pm = x_0^\pm$ and the interval \bar{C} . **Left** and **Middle** : The local operator is spatially separated from \bar{C} . In this case, the non-trivial part of the CFT entropy ΔS in the generalized entropy is vanishing due to causality. **Right**: When the local operator and the \bar{C} are causally connected, the right mover emitted by the quench can enter the causal diamond of $D[\bar{C}]$. Only in this case, ΔS is non vanishing.

an entangled pair of particles. Then the CFT entropy can be non-trivial only when one of these shock waves enters the causal diamond of the region $D[\bar{C}]$, whereas its partner does not. Therefore, for the fixed end point of the subsystem, $x^\pm = x_5^\pm$, we have four possible behaviors of the entropy, according to the location of the local operator relative to the end point as in figure 7.

(1) When the end point x_5 is in the right wedge of the location of the operator x_0 , ie, $x_5^\pm > x_0^\pm$, both left mover and right mover do not enter the causal diamond $D[\bar{C}]$ of the subsystem \bar{C} . Therefore, the shock wave can not affect the state on the subsystem \bar{C} , the entanglement entropy remains unchanged due to causality.

(2) Similarly when the end point is in the left wedge of the insertion $x_0^\pm > x_5^\pm$, both shock waves enter the causal diamond, and the entanglement entropy again remains unchanged.

(3) When the local operator is in the future or past of the end point, the entanglement entropy can be non-trivial. When it is in the future light cone of the end point x_5 , ie $x_5^- > x_0^-$ and $x_0^+ > x_5^+$, then only the left moving shock contributes to the entropy. The difference between this entanglement entropy and the thermal one $\Delta S \equiv S_{\beta,E}[\bar{C}] - S_\beta[\bar{C}]$ is given by [51]

$$\Delta S_F = \frac{c}{6} \log \left[\frac{\beta}{\pi \varepsilon} \frac{\sin \pi \alpha}{\alpha} \frac{\sinh \frac{\pi}{\beta} (x_0^+ - x_5^+) \sinh \frac{\pi}{\beta} (x_6^+ - x_0^+)}{\sinh \frac{\pi}{\beta} (x_6^+ - x_5^+)} \right]. \quad (4.17)$$

When the operator is in the past light cone of the end point, $x_0^- > x_5^-$ and $x_5^+ > x_0^+$, then only the right mover contributes, and the entropy difference is

$$\Delta S_P = \frac{c}{6} \log \left[\frac{\beta}{\pi \varepsilon} \frac{\sin \pi \alpha}{\alpha} \frac{\sinh \frac{\pi}{\beta} (x_0^- - x_5^-) \sinh \frac{\pi}{\beta} (x_6^- - x_0^-)}{\sinh \frac{\pi}{\beta} (x_6^- - x_5^-)} \right]. \quad (4.18)$$

4.3.2 CFT entropy for two disjoint intervals

In the actual calculations of the generalized entropy, we need an expression of the CFT entanglement entropy for two disjoint intervals $\bar{C} = \bar{C}_1 \cup \bar{C}_2$. Again, the behavior of the entanglement entropy is strongly constrained by causality. In the previous section, we saw that these two intervals become smaller and smaller $\bar{C}_1, \bar{C}_2 \rightarrow 0$ in the high temperature limit $\beta \rightarrow 0$. This means that the entropy of this two disjoint intervals gets factorized,

$$S[\bar{C}] = S[\bar{C}_1] + S[\bar{C}_2]. \quad (4.19)$$

so the result for the single interval is enough to fix the generalized entropy in this limit. For simplicity, we assume the shock wave does not intersect the left interval \bar{C}_1 , ie x_0^\pm , so only the entropy of the right interval $S[\bar{C}_2]$ can change non-trivially.

4.4 Quantum extremal surfaces

We are interested in, how the dominant quantum extremal surface changes as we tune the location of the operator x_0 . We are especially interested in the high temperature limit $\beta \rightarrow 0$, where the classical horizon is getting close to the infinity $x^\pm = \frac{\pi}{2}$. It is convenient to decompose the CFT entropy $S_{\beta,E}[\bar{C}] - S_{\text{vac}}[\bar{C}]$ in (4.2), into the trivial part $S_\beta[\bar{C}] - S_{\text{vac}}[\bar{C}]$ which does not involve the shock wave, and the non-trivial part $\Delta S = S_{\beta,E}[\bar{C}] - S_\beta[\bar{C}]$. Then the trivial part does not play any role in the generalized entropy in the high temperature limit. As we saw in the previous section, the classical extremal surfaces in this limit are given by the bifurcation surfaces of the black hole. Therefore, we can focus on the non-trivial part of the CFT entropy to find the quantum extremal surfaces. Without going into detail, let us describe two limiting cases.

First, when the insertion is made in the deep interior of the black hole $x_0 \sim 0$, the true quantum extremal surface almost coincides with the classical horizon of the deformed black hole (The one with back-reaction of the shock wave) at $x^\pm = x_H^\pm(E)$, defined in (4.12). This is because the local operator is spatially separated from the horizon, so the non-trivial part of the CFT entropy ΔS is vanishing due to causality.

On the other hand, if the operator is inserted at the exterior of the horizon, ie $x_0 > x_H(E)$, then, since again the non-trivial part of the CFT entropy is vanishing, the QES coincides with the classical extremal surface, which is identified with the horizon of the original black hole (ie, black hole without the shock wave) at $x^\pm = x_H^\pm(0)$ (4.11). Below, we discuss details of the dynamics of the QESs.

We remark that the generalized entropies also have the contribution from the the left classical extremal surface, which is independent of the location of the operator as long as the operator is inserted at the region $x_0^+ + x_0^- > 0$. The contribution from the left extremal surface is given by (3.14) in the high temperature limit and let us denote it by S_L . Then, the generalized entropies for each case are given as follows.

Case 1

When the local operator is inserted inside of the original horizon (the left panel of figure 7), $x_0 < x_H(0)$, the quantum extremal surface coincides with the bifurcation surface of the deformed black hole at $x^\pm = x_H(E)$. Also, since $\Delta S = 0$ in this case, we get the following expression for the generalized entropy,

$$\begin{aligned} S_{\text{gen}} &= \Phi_{\beta,E}(x_H(E)) + S_L \\ &= \phi_0 - \frac{4}{\Lambda} \left[\left(\frac{\pi X_\beta}{2} \right)^2 + \pi X_\beta E \cos^2 x_0 \right] - \frac{4}{\Lambda} E^2 \cos^4 x_0 + 2E \cos^2 x_0 \tan x_0 + S_L. \end{aligned} \quad (4.20)$$

Case 2

When we insert the operator in between two bifurcation surfaces (the middle panel of figure 7), $x_H(0) < x_0 < x_H(E)$, the generalized entropy is given by

$$\begin{aligned} S_{\text{gen}} &= \min \{ \Phi_\beta(x_H(0)), \Phi_{\beta,E}(x_H(E)) \} + S_L \\ &= \phi_0 - \frac{(\pi X_\beta)^2}{\Lambda} + \min \left\{ 0, -2E \cos^2 x_0 \left(\frac{2\pi X_\beta}{\Lambda} + \frac{2}{\Lambda} E \cos^2 x_0 - \tan x_0 \right) \right\} + S_L. \end{aligned} \quad (4.21)$$

Again in this case the non-trivial part of the CFT entropy ΔS vanishes.

The transition point $x^\pm = x_T$, at which the dominance in the minimization of the above expression changes, satisfies the equation

$$\tan x_T = \frac{2\pi X_\beta}{\Lambda} + \frac{2}{\Lambda} E \cos^2 x_T. \quad (4.22)$$

Case 3

When the operator is inserted at the outside of the deformed horizon (the right panel of figure 7), $x_H(E) < x_0$, we have

$$\begin{aligned} S_{\text{gen}} &= \Phi_\beta(x_H(0)) + S_L \\ &= \phi_0 - \frac{(\pi X_\beta)^2}{\Lambda} + S_L. \end{aligned} \quad (4.23)$$

Net result

By combining above results, we get the generalized entropy in the high temperature limit as the function of x_0 ,

$$S_{\text{gen}}(x_0) = \begin{cases} \phi_0 - \frac{(\pi X_\beta)^2}{\Lambda} - 2E \cos^2 x_0 \left(\frac{2\pi X_\beta}{\Lambda} + \frac{2}{\Lambda} E \cos^2 x_0 - \tan x_0 \right) + S_L & \text{for } x_0 < x_T \\ \phi_0 - \frac{(\pi X_\beta)^2}{\Lambda} + S_L & \text{for } x_T < x_0. \end{cases} \quad (4.24)$$

We plot the above generalized entropy for several values of E in figure 8³.

From the plot we see that when the operator is in the exterior of the horizon, the generalized entropy does not change. On the other hand, when it is inserted in the black hole interior always make the entropy decrease. Also we observe that, as the location of the local operator goes deeper interior of the black hole, the entropy gets significantly decreased. This is because if the shock wave is created inside of the horizon, it makes the interior wormhole region longer (which is seen from the relation $x_H(0) < x_H(E)$), and reduces the entropy of the black hole $\Phi_\beta(x_H(0)) > \Phi_{\beta,E}(x_H(E))$. Therefore, in some sense what the shock wave does is to make the black hole further “evaporate”. This black hole in the universe B has been evaporating due to the entanglement with the non-gravitating universe A, and the insertion of the local operator accelerates the evaporation, which leads to the faster decrease of the entropy.

The actual entanglement entropy $S(\rho_A)$ is given by the minimum between $S_{\text{no-island}}$ and $S_{\text{gen}}(x_0)$. We plot this curve in figure 9. Since we are interested in how this $S(\rho_A)$ changes as we increase the entanglement temperature $1/\beta$, we plot it as a function of $1/\beta$ while the location of the operator $x^\pm = x_0^\pm$ is kept fixed. As we increase the entanglement temperature, the bifurcation surface of the black hole approaches the asymptotic infinity, and the operator at $x^\pm = x_0^\pm$ is eventually absorbed into the black hole. We again observe that above some critical temperature, the entanglement entropy is dominated by the generalized entropy $S_{\text{gen}}(x_0)$ (4.24). In the high temperature limit, since the operator goes into deep interior of the black hole, $S_{\text{gen}}(x_0)$ is given by the first line of (4.24). Therefore an approximate

³The plots shown in this paper are obtained by full numerical calculations by faithfully extremizing the generalized entropies, on the contrary to analytical expressions appear in the body of the paper.

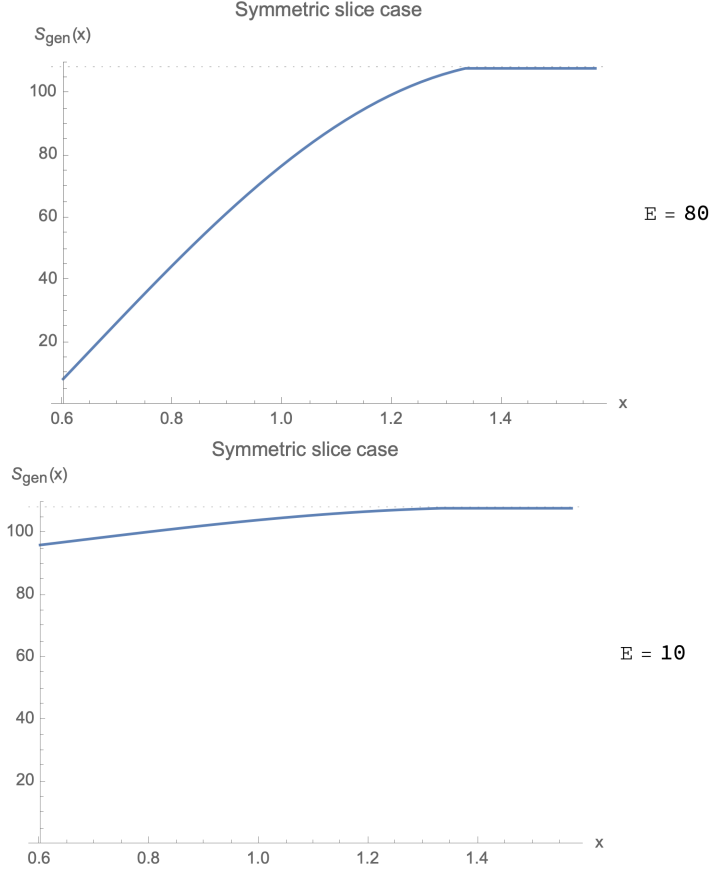


Figure 8: Plots of S_{gen} , (4.24), as the function of x_0 ($0 \leq x_0 \leq \pi/2$) with $\phi_0 = 1700$, $\beta = 1$, $\Lambda = 500$, $c = 50$, $\varepsilon = 0.1$. $\Delta = 8$ ($E = 80$)(top) and $\Delta = 1$ ($E = 10$)(bottom). The dotted line is the value of the entropy for the shock-less case, $\Delta = 0$ ($E = 0$).

expression for the entanglement entropy reads,

$$S(\rho_A) = \begin{cases} S_{\text{no-island}} = \frac{\pi^2 c}{3\beta} & \beta \gg \beta_c \\ S_{\text{gen}}(x_0) = \phi_0 - \frac{(\pi X_\beta)^2}{\Lambda} - 2E \cos^2 x_0 \left(\frac{2\pi X_\beta}{\Lambda} + \frac{2}{\Lambda} E \cos^2 x_0 - \tan x_0 \right) + S_L & \beta \ll \beta_c. \end{cases} \quad (4.25)$$

It is interesting to compare this result with the Page curve without the operator insertion (3.16). In this case, above the critical temperature the entropy decreases as

$$S_{\text{island}} = \phi_0 - \frac{(\pi X_\beta)^2}{\Lambda} + S_L. \quad (4.26)$$

By comparing it with (4.25), we see that the entropy in the presence of the shock wave is reduced faster than the entropy without the shock, by increasing the entanglement tempera-

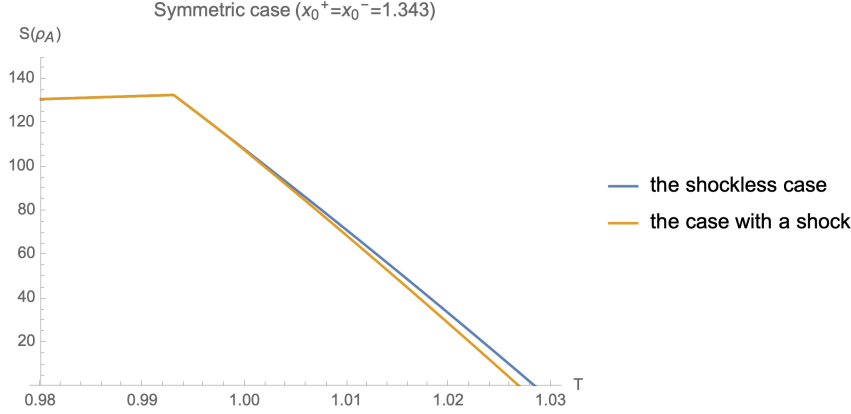


Figure 9: Plots of the Page curves corresponding to the shockless case (3.16) and the case with a shock (4.25) as the function of $T = 1/\beta$ with fixing the position of the operator, which we place on the reflection symmetric slice $x_0^+ = x_0^-$. $\phi_0 = 1700$, $\Lambda = 500$, $c = 50$, $\Delta = 10$, $\varepsilon = 0.01$, $x_0^+ = x_0^- = 1.343$. The island begins dominating at $T \simeq 0.993$ and the location of the corresponding QES is $x_H^+(0) = x_H^-(0) \simeq 1.328$. The entanglement entropy with a shock decreases faster than the one without it.

ture. This also supports the point of view that the shock wave accelerates the evaporation of the black hole.

4.5 QESs with non-trivial CFT entropy

In the above examples, the CFT entropy did not play any role. This is because, when the operator is inserted on the time reflection symmetric slice $x_0^+ = x_0^-$, the quantum extremal surfaces and the local operator are always spatially separated, therefore the non-trivial part of the CFT entropy $\Delta S = S_{\beta,E}[\bar{C}] - S_{\beta}[\bar{C}]$ vanishes in the generalized entropy. As a result, the QESs coincide with the classical extremal surfaces, which can be identified with the bifurcation surfaces of the black hole. On the other hand, when we insert the operator in the future light cone of the original horizon $x^\pm = x_H^\pm(0)$, then the non-trivial part of the CFT entropy is non vanishing. In this case, we insert the local operator in the region $x_0^+ > x_H^+(0)$, $x_0^- < x_H^-(0)$. Let us first derive the location of the classical extremal surface. The dilaton profile is still given by (4.8), and since we expect the new bifurcation surface is in the past light cone of the operator, we extremize

$$\begin{aligned} \Phi_R(x^\pm) = & \phi_0 + \frac{\Lambda}{4} \tan x^+ \tan x^- - X_\beta(x^+ \tan x^+ + x^- \tan x^-) \\ & - E \cos^2 x_0^- (\tan x^- - \tan x_0^-). \end{aligned} \quad (4.27)$$

The critical point $(x_{\mathcal{H}}^+(E), x_{\mathcal{H}}^-(E))$ of this dilaton profile $\Phi_R(x^\pm)$ satisfies

$$x_{\mathcal{H}}^-(E) = x_H^-(0), \quad \tan x_{\mathcal{H}}^+(E) = \tan x_H^+(0) + \frac{4E}{\Lambda} \cos^2 x_0^-. \quad (4.28)$$

We remark that this is different from the critical point $(x_H^+(E), x_H^-(E))$ of $\Phi_{\beta,E}$ (4.10) discussed in the previous subsection.

The net effect of the shock wave is shifting the horizon along the x^+ direction. In order for this critical point $(x_{\mathcal{H}}^+(E), x_{\mathcal{H}}^-(E))$ to be really in the past light cone of the operator, we need,

$$\tan x_H^+(0) + \frac{4E}{\Lambda} \cos^2 x_0^- < \tan x_0^+. \quad (4.29)$$

Now let us add quantum effects. The expression of the generalized entropy can be obtained from (4.17),

$$S_{\text{gen}}(x^\pm) = \Phi_R(x^\pm) + \frac{c}{6} \log \left[\frac{\beta}{\pi \varepsilon} \frac{\sin \pi \alpha}{\alpha} \frac{\sinh \frac{\pi}{\beta}(x_0^+ - x_5^+) \sinh \frac{\pi}{\beta}(x_6^+ - x_0^+)}{\sinh \frac{\pi}{\beta}(x_6^+ - x_5^+)} \right] + S_\beta[\bar{C}] - S_{\text{vac}}[\bar{C}] + S_L \quad (4.30)$$

where S_L is the contribution of the left horizon, as in the previous subsection. In the high temperature limit, $S_L = \Phi_\beta(x_H^\pm(0))$ defined in (3.14).

We then specify the location of the quantum extremal surface $x^\pm = x_{Q_1}^\pm$ by finding the critical point of the above generalized entropy (4.30). Since its derivative along the x^- direction is not affected by the non-trivial part of the CFT entropy ΔS , $\tan x_{Q_1}^+$ is still given by

$$\tan x_{Q_1}^+ = \tan x_H^+(0) + \frac{4E}{\Lambda} \cos^2 x_0^-. \quad (4.31)$$

The derivative along the x^+ direction is modified by ΔS . By ignoring its trivial part $S_\beta[\bar{C}] - S_{\text{vac}}[\bar{C}]$, we get

$$\tan x_{Q_1}^- = \frac{4}{\Lambda} \left[\frac{\pi}{2} X_\beta + \frac{c\pi}{6\beta} \cos^2 x_{Q_1}^+ \left(\frac{1}{\sinh \frac{\pi}{\beta}(x_0^+ - x_{Q_1}^+)} - \frac{1}{\sinh \frac{\pi}{\beta}(x_6^+ - x_{Q_1}^+)} \right) \right]. \quad (4.32)$$

The contribution of this quantum extremal surface is given by plugging the solution of these equations (4.31) and (4.32) to the expression of the generalized entropy (4.30).

There is another quantum extremal surface, $x^\pm = x_{Q_2}^\pm$ located at the right wedge of the operator $x_{Q_2}^\pm > x_0^\pm$. In this case, the non-trivial part of the CFT entropy ΔS is vanishing, so it coincides with the bifurcation surface of the original black hole $x_{Q_2}^\pm = x_H^\pm(0)$.

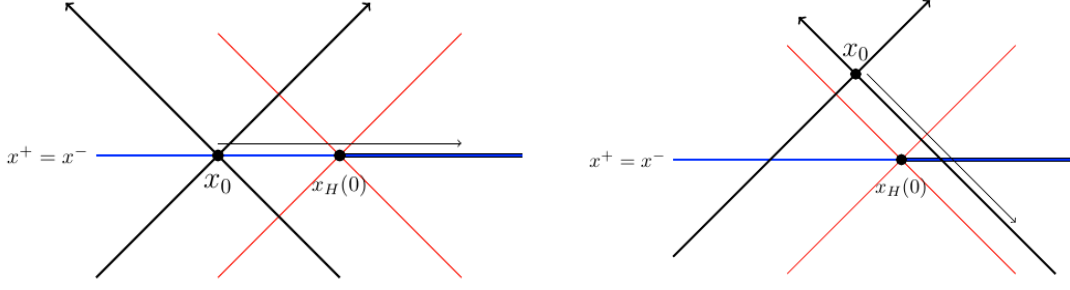


Figure 10: **Left:** The operator inserted on the time reflection symmetric slice (the blue line). In this case the operator is spatially separated from the bifurcation surface of the black hole at $x^\pm = x_H^\pm(0)$. (The black hole horizon is drawn by the red lines.) **Right:** The operator inserted on the non time reflection symmetric slice. In this case, the bifurcation surface can causally contact with the operator.

Although we have two candidates of the quantum extremal surface at $x^\pm = x_{Q_1}^\pm$ and $x^\pm = x_{Q_2}^\pm$, they can not appear simultaneously. This is due to the non-symmetric insertion of the local operator. If we put the local operator at the future light cone of the bifurcation surface of the original black hole $x_0^+ > x_H^+(0)$, $x_0^- < x_H^-(0)$, then the bifurcation surface is moved to $(x_{\mathcal{H}}^+(E), x_{\mathcal{H}}^-(E))$. In this case $x_H^\pm(0) = x_{Q_2}^\pm$ is no longer extremal, and only $x^\pm = x_{Q_1}^\pm$ is the quantum extremal surface. On the other hand, if the operator x_0^\pm is in the exterior of the horizon $x_0^\pm > x_H^\pm(0)$, then only $x^\pm = x_{Q_2}^\pm$ is the quantum extremal surface. Thereby, the generalized entropy is given by

$$S_{\text{gen,E}}(x_0^+, x_0^-) = \begin{cases} S_{\text{gen}}(x_{Q_1}^\pm) & \text{for } x_H^-(0) > x_0^- \\ S_{\text{gen}}(x_{Q_2}^\pm) & \text{for } x_H^-(0) < x_0^- \end{cases} \quad (4.33)$$

In the high temperature limit, $S_{\text{gen}}(x_{Q_1}^\pm)$ is obtained by plugging the solution of (4.32) into (4.30). $S_{\text{gen}}(x_{Q_2}^\pm)$ coincides with the entropy of the original black hole $\Phi_\beta(x_H^\pm(0))$. The actual entanglement entropy is given by the minimum between this generalized entropy and $S_{\text{no-island}}$,

$$S(\rho_A) = \min \{ S_{\text{no-island}}, S_{\text{gen,E}} \}. \quad (4.34)$$

Plot of the result

Let us focus on the case, where the location of the left mover $x^+ = x_0^+$ is fixed, but the location of the right mover $x^- = x_0^-$ is varied as in the right panel of figure 10. We also demand $x_0^+ > x_H^+(E)$, so that the location of the operator interpolates the interior and the exterior of the black hole. We plot the generalized entropy $S_{\text{gen,E}}(x_0^\pm)$ in figure 11. By decreasing the value of x_0^- , the local operator is falling to the black hole horizon, and we

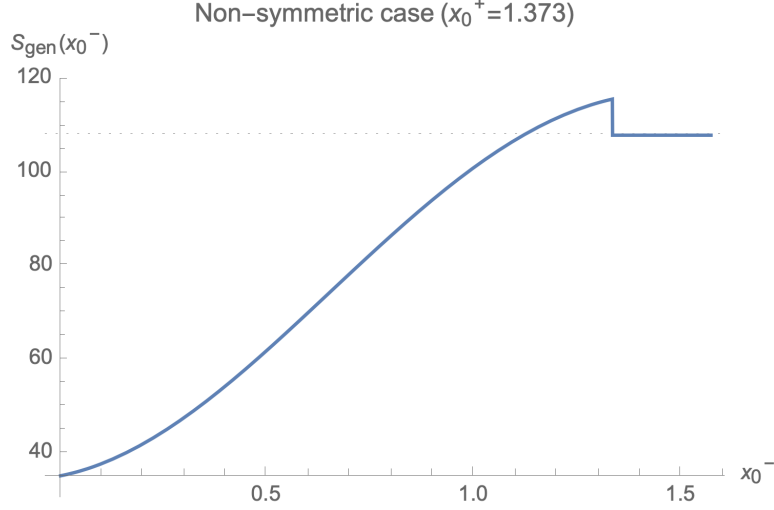


Figure 11: Plot of the generalized entropy given in (4.33) as a function of x_0^- with x_0^+ kept fixed (the case of the non-symmetric insertion), with the choice of parameters $\phi_0 = 1700$, $\Lambda = 500$, $c = 50$, $\beta = 1$, $\Delta = 7$, $\varepsilon = 0.1$, $x_0^+ = 1.373$. The dotted line corresponds to the shockless case $\Delta = 0$.

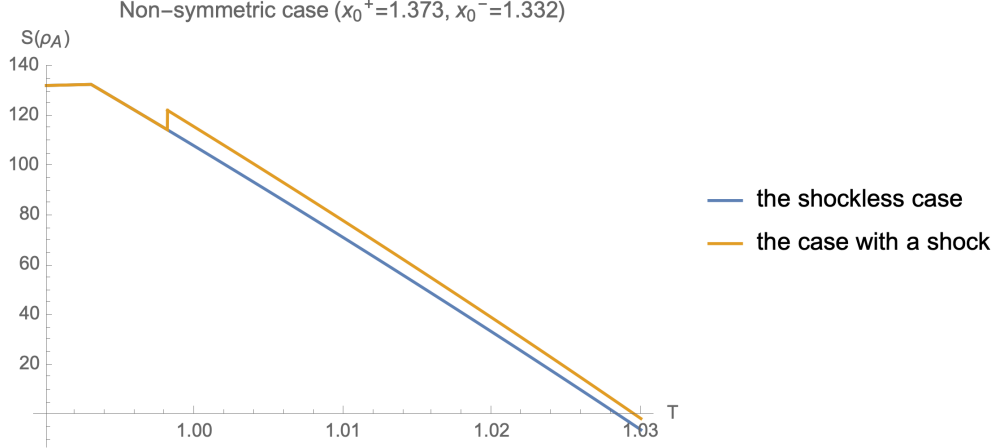


Figure 12: Plots of the Page curves corresponding to the shockless case (3.16) and the case with a shock wave (4.34) as the function of $T = 1/\beta$ with fixing the position of the operator, which is not on the reflection symmetric slice, ie $x_0^+ \neq x_0^-$, with the choice of parameters $\phi_0 = 1700$, $\Lambda = 500$, $c = 50$, $\Delta = 7$, $\varepsilon = 0.1$, $x_0^+ = 1.373$, $x_0^- = 1.332$. The island begins dominating at $T \simeq 0.993$ and the location of the corresponding QES is $x_H^+(0) = x_H^-(0) \simeq 1.328$.

are interested in, how the entropy changes as the local operator is falling to the horizon and eventually enters the interior⁴.

⁴In studying the Page curve for an evaporating black hole, the setup where an AdS black hole is attached to a non-gravitating heat bath at the asymptotic boundary is often used, for example in [2, 58, 59]. In such

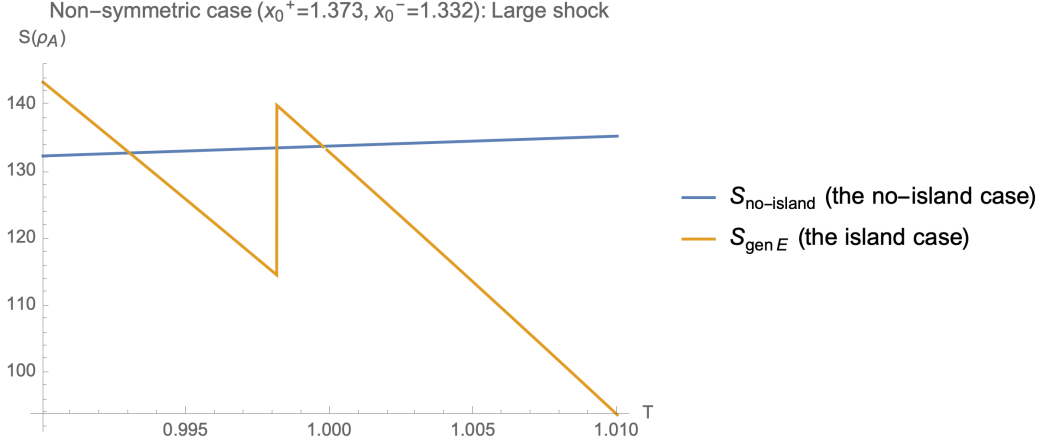


Figure 13: Similar plot to figure 12 but the shock wave has a larger energy than the previous case. We plot the Page curve only around the points at which the non-trivial dominance changes happen unlike the previous case (figure 12). The Page curve is given by the minimum of them. We set the parameters to $\phi_0 = 1700$, $\Lambda = 500$, $c = 50$, $\Delta = 8$, $\varepsilon = 0.01$, $x_0^+ = 1.373$, $x_0^- = 1.332$. In this case, the transitions between them happen several times. The first transition is at $T \simeq 0.993$ and the location of the corresponding QES is $x_H^+(0) = x_H^-(0) \simeq 1.328$.

This plot in figure 11 for the asymmetric insertion is compared to the similar plot shown in figure 8, where we insert the operator on the time reflection symmetric slice (4.24), as in the left panel of figure 10. These two plots share a common feature. Namely, when the operator is inserted outside of the horizon $x^- > x_H^-(0)$, the values of these two entropies both approach the classical entropy of the original black hole $\Phi_\beta(x_H^\pm(0))$, defined in (3.14). This happens because, the non-trivial part of the CFT entropy ΔS vanishes since the local operator is in the causal diamond of \bar{C} .

However these two generalized entropies behave differently when the operator is inserted in the black hole interior $x_0^- < x_H^-(0)$. In particular, there is a bump in the entropy plot for the asymmetric insertion in figure 11, which is absent in the plot for the symmetric insertion 8. This difference is a direct consequence of the fact that the quantum extremal surface for the asymmetric insertion is in the past of the local operator, so the non-trivial part of the CFT entropy ΔS is non vanishing. On the other hand, in the case of the symmetric insertion, the QES is spatially separated from the local operator, so ΔS is vanishing.

This bump in figure 11 can be understood as a result of the dynamics of the black hole.

a setup, the local operator itself is inserted in the (non-gravitating) bath region, and the shock wave created by the operator can enter the bulk region. Instead, in our setup, we insert the operator in the gravitating universe, and the operator itself can enter the black hole interior. We regard our shock waves as a kind of ‘heavy diaries’, ex.[3, 58, 60].

For this purpose, it is useful to follow the plot backward in the x_0^- direction. By decreasing x_0^- , the black hole gets bigger due to its absorption of the local operator, and this causes the sudden increase of the entropy in the plot. After the increase of its size, the black hole starts to evaporate again, and as a result, the generalized entropy starts decreasing.

One can characterize the difference between these two generalized entropies, by the difference of the natures of these two insertions. The symmetric insertion can be regarded as a local operation, because in this case the local operator is always in either the causal diamond of the island $D[C]$ (which can be regarded as a part of the radiation system) or the entanglement wedge of the black hole $D[\bar{C}]$, as in the left panel of figure 10. Since they are LOCCs, they can only decrease the entanglement entropy. On the other hand, operators inserted asymmetrically enter a region of the black hole interior, which does not belong to neither of these two entanglement wedges (the right panel of figure 10). Therefore, these insertions are not LOCCs, so they can increase the entanglement between two wedges.

4.6 The entanglement entropy

The entanglement entropy $S(\rho_A)$ is given by putting these results to the formula (4.34). Again we plot this as a function of the entanglement temperature $1/\beta$ with the location of the operator $x^\pm = x_0^\pm$ kept fixed in figure 12 and 13. As we increase temperature, the horizon expands, and the local operator is absorbed into the black hole. So also in this case, we can see the identical physics which leads to the result obtained by varying x_0^- .

When the location of the operator is properly chosen, the resulting entanglement entropy behaves in a complicated manner as in 13. This is compared to the same entropy without the shock wave (3.16), where the transition between $S_{\text{no-island}}$ and S_{island} happens only once. Instead, in the presence of the shock, the transition can happen multiple times. In the actual plot in figure 13, we observe that at sufficiently low temperature, $S_{\text{no-island}}$ dominates, and by increasing the entanglement temperature S_{island} becomes the dominant one, as we can also see in the case without the shock wave. However, this is not the end of the story. Namely further increase of the temperature makes the horizon expand, so the local operator is falling to the horizon. This will lead to the size change of the black hole, and to the sudden increase of S_{island} . Now this S_{island} gets larger than the naive Hawking's entropy, so above this temperature $S_{\text{no-island}}$ again dominates. After this, the size of the black hole is eventually reduced due to the emissions of Hawking quanta, so eventually S_{island} gets smaller than $S_{\text{no-island}}$, and it becomes dominant once again.

5 Conclusion

In this paper, we studied dynamics of black holes in flat space, when it is entangled with an auxiliary non-gravitating universe. We find the back-reaction of the entanglement between them reduces the horizon area of the black hole, and lengthening its interior region. This lengthening can be understood in terms of monogamy property of entanglement [28]. Since the gravitating universe B contains two horizons, the Hilbert space of B can be naturally decomposed into two horizon Hilbert spaces $H_{B_L} \otimes H_{B_R}$. Since both of these degrees of freedom are strongly entangled with H_A , the entanglement between two horizons should be suppressed, according to monogamy of entanglement. This suppression is geometrized by the long interior region of the black hole. We then computed the entanglement entropy between the two universes, and found a Page curve for an evaporating black hole.

We also studied actions of local operations on the black hole. Such a local operation is modeled by an insertion of a CFT operator. In our setup, it is natural to consider the insertions in the black hole interior, in addition to the ones in the exterior. This insertion can back-react to the black hole through its stress energy tensor. The (quantum) extremal surfaces in the back-reacted black hole highly depend on the location of the insertion. There are several differences between the insertions in the interior and exterior. When the operator is in the exterior of the black hole, it does not change the entanglement entropy. On the other hand, the entropy is significantly reduced when the operator is in the interior. The disruption becomes stronger as the location of the insertion gets deeper in the interior of the black hole.

It would be interesting to study how can an observer in the non-gravitating universe A recover the information of shock wave in the black hole interior in the gravitating universe B. One way to do so is using the modular flow of the reduced density matrix ρ_A . Our setup is especially suitable for this purpose. This is because these two universes can be embedded in the larger Minkowski space, in which AB are both realized as the left and right wedges of the origin. Furthermore, the TFD state on AB is identified with the vacuum of this larger Minkowski space. By focus on the code subspace, the modular Hamiltonian of ρ_A is approximated by the CFT vacuum modular Hamiltonian of the CFT on AC , $-\log \rho_A = K_{AC}^{\text{CFT}}$, where C is the island region in the gravitating universe B [64]. In a CFT with a large central charge and a sparse spectrum, this modular Hamiltonian is given by the sum of two modular Hamiltonians for single intervals, each of which connects the endpoints of A and C. In 2d CFT, this vacuum modular Hamiltonian has a particularly simple form, as an integral of stress energy tensor. Since this modular flow is geometric, one can visualise how an operator in the black hole interior gets out of the horizon under the flow.

Acknowledgement

TU thanks Vijay Balasubramanian, Arjun Kar and Kotaro Tamaoka for useful discussions in the related projects. TU was supported by JSPS Grant-in-Aid for Young Scientists 19K14716.

A Entanglement entropy and local quench for two disjoint intervals

In this appendix we derive the results presented in 4.3.1 and 4.3.2 for the CFT entanglement entropy in the presence of a local operator insertion, by following the argument of [51]. We are interested in the state (4.1) of the total system AB , and its reduced density matrix on two disjoint intervals \bar{C} in the universe B . In the body of this paper, this region \bar{C} is identified with the compliment of the island C in the universe B .

Let $\rho_{\bar{C}}$ denote the reduced density matrix on two disjoint intervals $\bar{C} = \bar{C}_1 \cup \bar{C}_2$, whose endpoints are given by x_2^\pm and x_3^\pm ($x_2^\pm \leq x_3^\pm$) for \bar{C}_1 and x_5^\pm and x_6^\pm ($x_5^\pm < x_6^\pm \leq x_6^\pm$) for \bar{C}_2 respectively(see figure 14), that is, $\rho_{\bar{C}} = \text{tr}_C \rho$, where ρ is given by the reduced density matrix of the universe B (4.3). The CFT entanglement entropy of the density matrix can be calculated by using the replica trick. For this purpose, we first consider the n -th Rényi entanglement entropy

$$S^{(n)}[\bar{C}] \equiv \frac{1}{1-n} \log \text{tr} \rho_{\bar{C}}^n \quad (\text{A.1})$$

and, by taking the limit

$$S[\bar{C}] = \lim_{n \rightarrow 1} S^{(n)}[\bar{C}], \quad (\text{A.2})$$

we obtain the CFT entanglement entropy.

To evaluate $\text{tr} \rho_{\bar{C}}^n$, we need to compute a normalized $2n$ -point function on an n -sheeted replica manifold branched along the \bar{C} . Since the reduced density matrix $\rho_{\bar{C}}$ has the thermal form, each replica sheet is a cylinder with the period β . This $2n$ -point function is identical to the normalized six-point function including twist operators on a (no-replicated) manifold (thermal cylinder), in the cyclic orbifold theory $CFT^{\otimes n}/Z_n$. We adopt the later description and compute the six-point function

$$\text{tr} \rho_{\bar{C}}^n = \frac{\langle \mathcal{O}^{\otimes n}(x_1^+, x_1^-) \sigma_n(x_2^+, x_2^-) \sigma_{-n}(x_3^+, x_3^-) \sigma_n(x_5^+, x_5^-) \sigma_{-n}(x_6^+, x_6^-) \mathcal{O}^{\dagger \otimes n}(x_4^+, x_4^-) \rangle_\beta}{(\langle \mathcal{O}(x_1^+, x_1^-) \mathcal{O}^\dagger(x_4^+, x_4^-) \rangle_\beta)^n}, \quad (\text{A.3})$$

where $\langle \cdots \rangle_\beta$ means the thermal trace $\text{tr}[\rho_\beta \cdots]$.

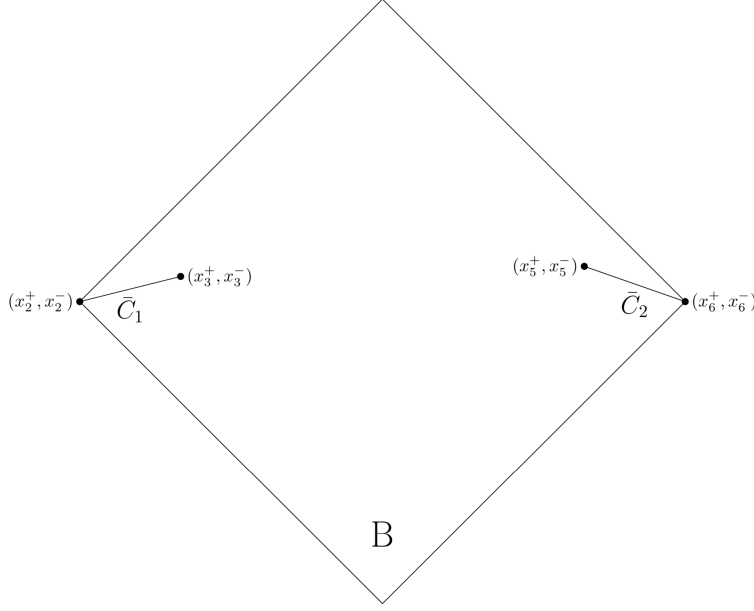


Figure 14: The two intervals in the universe B

In the above correlation function, we introduced the UV regulator ε in the location of the operators as follows,

$$\begin{cases} x_1^\pm = x_0^\pm \mp i\varepsilon, \\ x_4^\pm = x_0^\pm \pm i\varepsilon; \end{cases} \quad (\text{A.4})$$

$\mathcal{O}^{\otimes n}$ and $\mathcal{O}^{\dagger \otimes n}$ represent the products of the operators \mathcal{O}_i and \mathcal{O}_i^\dagger which are the i -th copies of the operators in the cyclic orbifold theory,

$$\begin{aligned} \mathcal{O}^{\otimes n} &= \mathcal{O}_1 \mathcal{O}_2 \dots \mathcal{O}_n, \\ \mathcal{O}^{\dagger \otimes n} &= \mathcal{O}_1^\dagger \mathcal{O}_2^\dagger \dots \mathcal{O}_n^\dagger. \end{aligned} \quad (\text{A.5})$$

with the conformal dimension $nh_{\mathcal{O}}$; σ_n and σ_{-n} are twist and anti-twist fields respectively with the conformal dimension $2H_n$,

$$H_n = \frac{c}{24} \left(n - \frac{1}{n} \right). \quad (\text{A.6})$$

We will compute the six-point function (A.3) in a conformal field theory with gravity dual. Such a CFT has a large central charge and a sparse spectrum. In this class of theories, one can approximate the correlation function by a six-point Virasoro vacuum conformal block with an appropriate choice of branch, following the argument of [51]. In doing so, it is convenient

to map the thermal cylinder to a plane by

$$w^\pm(x^\pm) = \exp\left(\frac{2\pi}{\beta}(x^\pm - x_0^\pm)\right) \quad (\text{A.7})$$

and additionally apply a conformal transformation

$$z^\pm(w^\pm) = \frac{(w_1^\pm - w^\pm) w_{34}^\pm}{w_{13}^\pm (w^\pm - w_4^\pm)}, \quad (\text{A.8})$$

where we use the notation $w_{ij}^\pm = w_i^\pm - w_j^\pm$. By the conformal map $w^\pm \rightarrow z^\pm$, one can relate $\text{tr } \rho_C^n$ in (A.3) to the correlator on the plane,

$$\begin{aligned} \text{tr } \rho_C^n &= ((1 - z^+)(1 - z^-))^{2H_n} (z_{65}^+ z_{65}^-)^{2H_n} \\ &\times \left\{ \left(\frac{\beta}{\pi \varepsilon_{UV}} \right)^4 \sinh\left(\frac{\pi}{\beta} x_{65}^+\right) \sinh\left(\frac{\pi}{\beta} x_{65}^-\right) \sinh\left(\frac{\pi}{\beta} x_{32}^+\right) \sinh\left(\frac{\pi}{\beta} x_{32}^-\right) \right\}^{-2H_n} \\ &\times \langle \mathcal{O}^{\otimes n} | \sigma_n(z^+, z^-) \sigma_{-n}(1, 1) \sigma_n(z_5^+, z_5^-) \sigma_{-n}(z_6^+, z_6^-) | \mathcal{O}^{\otimes n} \rangle, \end{aligned} \quad (\text{A.9})$$

where we introduce the UV cutoff ε_{UV} and the notation

$$\begin{aligned} &\langle \mathcal{O}^{\otimes n} | \sigma_n(z^+, z^-) \sigma_{-n}(1, 1) \sigma_n(z_5^+, z_5^-) \sigma_{-n}(z_6^+, z_6^-) | \mathcal{O}^{\otimes n} \rangle \\ &\equiv \lim_{z_4^+, z_4^- \rightarrow \infty} (z_4^+ z_4^-)^{2nh_O} \langle \mathcal{O}^{\dagger \otimes n}(z_4^+, z_4^-) \sigma_n(z^+, z^-) \sigma_{-n}(1, 1) \sigma_n(z_5^+, z_5^-) \sigma_{-n}(z_6^+, z_6^-) \mathcal{O}^{\otimes n}(0, 0) \rangle. \end{aligned} \quad (\text{A.10})$$

Next, we evaluate (A.10) with an insertion of a complete set as follows

$$\begin{aligned} &\langle \mathcal{O}^{\otimes n} | \sigma_n(z^+, z^-) \sigma_{-n}(1, 1) \sigma_n(z_5^+, z_5^-) \sigma_{-n}(z_6^+, z_6^-) | \mathcal{O}^{\otimes n} \rangle \\ &= \sum_{\alpha} \langle \mathcal{O}^{\otimes n} | \sigma_n(z^+, z^-) \sigma_{-n}(1, 1) | \alpha \rangle \langle \alpha | \sigma_n(z_5^+, z_5^-) \sigma_{-n}(z_6^+, z_6^-) | \mathcal{O}^{\otimes n} \rangle, \end{aligned} \quad (\text{A.11})$$

where the sum runs over all possible intermediate states. However, in the $\varepsilon \rightarrow 0$ limit, z^\pm approach 1, and since the OPE $\sigma_n(z)\sigma_{-n}(1)$ starts from the identity, one can approximate the six-point function as a product of four-point functions,

$$\begin{aligned} &\langle \mathcal{O}^{\otimes n} | \sigma_n(z^+, z^-) \sigma_{-n}(1, 1) \sigma_n(z_5^+, z_5^-) \sigma_{-n}(z_6^+, z_6^-) | \mathcal{O}^{\otimes n} \rangle \\ &\simeq \langle \mathcal{O}^{\otimes n} | \sigma_n(z^+, z^-) \sigma_{-n}(1, 1) | \mathcal{O}^{\otimes n} \rangle \langle \mathcal{O}^{\otimes n} | \sigma_n(z_5^+, z_5^-) \sigma_{-n}(z_6^+, z_6^-) | \mathcal{O}^{\otimes n} \rangle, \end{aligned} \quad (\text{A.12})$$

in the $\varepsilon \rightarrow 0$ limit. By further applying a conformal map

$$\tilde{z}^\pm(z^\pm) = \frac{(z_1^\pm - z^\pm) z_{64}^\pm}{z_{16}^\pm (z^\pm - z_4^\pm)} \quad (\text{A.13})$$

to the second four-point function in (A.12), we get

$$\begin{aligned}
& \text{tr } \rho_{\bar{C}}^n(t) \\
&= \left\{ \left(\frac{\beta}{\pi \varepsilon_{UV}} \right)^4 \sinh \left(\frac{\pi}{\beta} x_{65}^+ \right) \sinh \left(\frac{\pi}{\beta} x_{65}^- \right) \sinh \left(\frac{\pi}{\beta} x_{32}^+ \right) \sinh \left(\frac{\pi}{\beta} x_{32}^- \right) \right\}^{-2H_n} \\
&\quad \times ((1-z^+)(1-z^-))^{2H_n} \langle \mathcal{O}^{\otimes n} | \sigma_n(z^+, z^-) \sigma_{-n}(1, 1) | \mathcal{O}^{\otimes n} \rangle \\
&\quad \times ((1-\tilde{z}_5^+)(1-\tilde{z}_5^-))^{2H_n} \langle \mathcal{O}^{\otimes n} | \sigma_n(\tilde{z}_5^+, \tilde{z}_5^-) \sigma_{-n}(1, 1) | \mathcal{O}^{\otimes n} \rangle.
\end{aligned} \tag{A.14}$$

Generally, it is difficult to get a complete analytic expression of the four-point functions since they depend on the details of the dynamics of the theory. However, because we focus on the theory that has the large central charge $c \gg 1$ and the sparse spectrum, the four-point functions can be well approximated by the vacuum Virasoro conformal blocks. Moreover, in evaluating the entanglement entropy by taking $n \rightarrow 1$ limit of the twist operators in the correlator (A.14), we only need the Heavy-Heavy-Light-Light Virasoro blocks, because the conformal dimension of the twist operators becomes light, $H_n \rightarrow 1, n \rightarrow 1$. Upon taking the limit, we keep the conformal dimension $h_{\mathcal{O}}$ of the local operator \mathcal{O} which we assume to be proportional to the central charge c fixed. The dominant contribution of such a four-point function under the limit is given by [65]

$$((1-z^+)(1-z^-))^{2H_n} \langle \mathcal{O}^{\otimes n} | \sigma_n(z^+, z^-) \sigma_{-n}(1, 1) | \mathcal{O}^{\otimes n} \rangle \simeq \left(\frac{(z^+)^{\frac{1-\alpha}{2}} (1-(z^+)^{\alpha}) (z^-)^{\frac{1-\alpha}{2}} (1-(z^-)^{\alpha})}{\alpha^2 (1-z^+)(1-z^-)} \right)^{-2H_n} \tag{A.15}$$

where $\alpha = \sqrt{1 - \frac{24h_{\mathcal{O}}}{c}} = \sqrt{1 - \frac{12\Delta}{c}}$. By plugging this result in (A.14) and taking $n \rightarrow 1$ limit, we get, the result for the CFT entanglement entropy $S[\bar{C}] = S_{\beta}[\bar{C}] + \Delta S[\bar{C}]$ with

$$\begin{aligned}
S_{\beta}[\bar{C}] &= \frac{c}{6} \log \left[\left(\frac{\beta}{\pi \varepsilon_{UV}} \right)^4 \sinh \left(\frac{\pi}{\beta} x_{65}^+ \right) \sinh \left(\frac{\pi}{\beta} x_{65}^- \right) \sinh \left(\frac{\pi}{\beta} x_{32}^+ \right) \sinh \left(\frac{\pi}{\beta} x_{32}^- \right) \right] \\
\Delta S[\bar{C}] &= \frac{c}{6} \log \left[\frac{(z^+)^{\frac{1-\alpha}{2}} (1-(z^+)^{\alpha}) (z^-)^{\frac{1-\alpha}{2}} (1-(z^-)^{\alpha})}{\alpha^2 (1-z^+)(1-z^-)} \right] \\
&\quad + \frac{c}{6} \log \left[\frac{(\tilde{z}_5^+)^{\frac{1-\alpha}{2}} (1-(\tilde{z}_5^+)^{\alpha}) (\tilde{z}_5^-)^{\frac{1-\alpha}{2}} (1-(\tilde{z}_5^-)^{\alpha})}{\alpha^2 (1-\tilde{z}_5^+)(1-\tilde{z}_5^-)} \right].
\end{aligned} \tag{A.16}$$

$S_{\beta}[\bar{C}]$ is the CFT entanglement entropy of the two disjoint intervals at finite temperature $T = 1/\beta$ and $\Delta S[\bar{C}]$ is the contribution to the CFT entanglement entropy from the perturbation by the local operator \mathcal{O} ⁵.

⁵Note that if we choose the other channel, then $S_{\beta}[\bar{C}]$ and $\Delta S[\bar{C}]$ take a different form.

The right hand side of the above formula (A.16) contains branch cuts, therefore to make it well-defined, we need to properly specify the branch. This is achieved by demanding that the resulting entanglement entropy is consistent with causality and positivity of $\Delta S[\bar{C}]$. In imposing these conditions, it is convenient to adopt the quasi-particle picture [47, 54, 55] for the time evolution of the entanglement entropy in a local quench. It claims the following: By a local quench, a pair of entangled quasi-particles is created, one of which is propagating along one spatial direction at the speed of light, and the other along propagates along the opposite direction.

The change of the CFT entanglement entropy $\Delta S[\bar{C}]$ can be non-zero only when one of such particles is in the \bar{C} while the other is not [47–57, 63]. This condition constrains possible branches, since vanishing of the entanglement entropy $\Delta S[\bar{C}] = 0$ is equivalent to choose the branch where $(z, z_5) \rightarrow 1$ in the $\varepsilon \rightarrow 0$ limit. If we have multiple branches satisfying the condition, the intuition coming from the dual holographic setup suggests that we should take the one giving the minimal value of $\Delta S[\bar{C}]$.

In our setup, the causality condition tells us that the CFT entanglement entropy is vanishing in the following three cases: (1) We insert the operator in the domain of dependence of the intervals, ie $x_0 \in D[\bar{C}_1]$ or $x_0 \in D[\bar{C}_2]$ (2) We do not insert the operator in these domains of dependence, but the right moving particle created by the quench enters $D[\bar{C}_2]$ and the left-mover enters $D[\bar{C}_1]$. (3) We insert the operator in $D[C]$, where C is the complement of \bar{C} .

More explicitly, the conditions that the CFT entanglement entropy must vanish in the above regions imply we should choose the branch $(z^+, z^-) \rightarrow (1, 1)$ and $(\bar{z}_5^+, \bar{z}_5^-) \rightarrow (1, 1)$ when the operator \mathcal{O} is inserted at

- (I) $D[\bar{C}_1]$: $x_0^+ < x_3^+, x_0^- < x_3^-$,
- (II) $D[\bar{C}_2]$: $x_5^+ < x_0^+, x_5^- < x_0^-$,
- (III) Union of the causal pasts of $D[\bar{C}_1]$ and $D[\bar{C}_2]$: $x_0^+ < x_3^+, x_5^- < x_0^-$,
- (IV) Union of the causal futures of $D[\bar{C}_1]$ and $D[\bar{C}_2]$: $x_5^+ < x_0^+, x_0^- < x_3^-$,
- (V) $D[C]$: $x_3^+ < x_0^+ < x_5^+, x_3^- < x_0^- < x_5^-$.

(See figure 15.)

The expression of $\Delta S[\bar{C}]$, when the operator is inserted in other regions, is given by suitable analytic continuations of (A.16) in x_0 from the above regions (I) – (V). By using

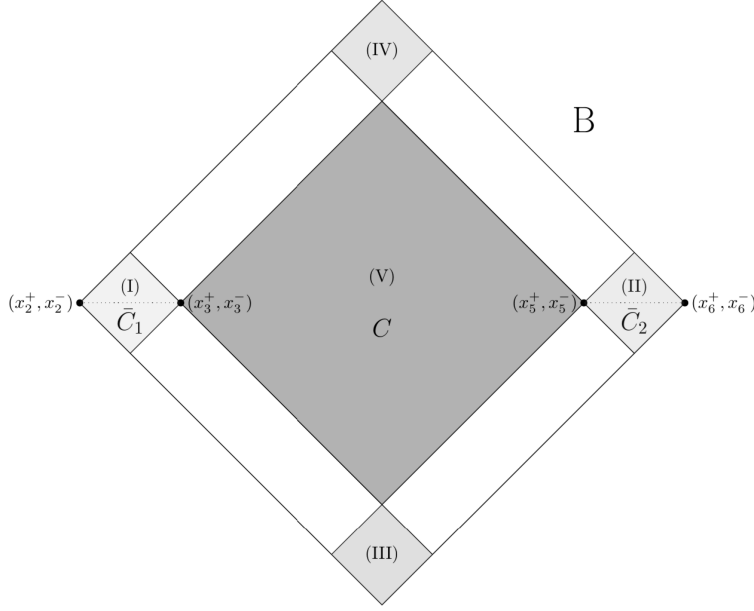


Figure 15: The regions in which $\Delta S[\bar{C}]$ must vanish. The shaded regions correspond to (I) – (V).

the above standard choices, we can determine branch cuts on the other regions from the consistency of analytic continuation for x_0^\pm .

We take the region $x_0^+ < x_3^+$ and $x_3^- < x_0^- < x_5^-$ as an example of such a calculation and determine possible branch choices in the region. Starting from the three regions (I), (III) and (V) which are adjacent to the region $x_0^+ < x_3^+$ and $x_3^- < x_0^- < x_5^-$, we move the operator \mathcal{O} to the region $x_0^+ < x_3^+$ and $x_3^- < x_0^- < x_5^-$. We expand z^\pm and \tilde{z}_5^\pm to the first order in ε , which is very small compared to β , and focus on the change of their imaginary parts under the move. For the case (I), the imaginary part of z^- changes sign from plus to minus at $x_0^- = x_3^-$, but the others not. In such case, we choose the branches as $(z^+, z^-) \rightarrow (1, e^{2\pi i})$ and $(\tilde{z}_5^+, \tilde{z}_5^-) \rightarrow (1, 1)$. For the case (III), the imaginary part of \tilde{z}_5^- changes sign from plus to minus $x_0^- = x_5^-$, but the others not. Similarly, we choose the branches as $(z^+, z^-) \rightarrow (1, 1)$ and $(\tilde{z}_5^+, \tilde{z}_5^-) \rightarrow (1, e^{2\pi i})$. For the case (V), the imaginary part of z^+ changes sign from minus to plus at $x_0^+ = x_3^+$, but the others not. In this case, we choose the branches as $(z^+, z^-) \rightarrow (e^{2\pi i}, 1)$ and $(\tilde{z}_5^+, \tilde{z}_5^-) \rightarrow (1, 1)$. By the above calculation, we have finished determining possible branch choices in the region $x_0^+ < x_3^+$ and $x_3^- < x_0^- < x_5^-$.

Having specified the branch cuts in the region, we can calculate the analytic expression for $\Delta S[\bar{C}]$ in the region. Since each branch cut gives a different $\Delta S[\bar{C}]$ and as noted before we must pick up the dominant contribution corresponding to the minimum $\Delta S[\bar{C}]$ in the region

[50]. For example, we focus on the region $x_0^+ < x_3^+$ and $x_3^- < x_0^- < x_5^-$, and calculate $\Delta S[\bar{C}]$. In this region, $x_0^+ < x_3^+$ and $x_3^- < x_0^- < x_5^-$, we must compare the above three branch choices obtained from the three regions, (I), (III) and (V), and choose the minimum one. This gives

$$\Delta S[\bar{C}] = \frac{c}{6} \log \left[\frac{\beta \sin \pi \alpha}{\pi \varepsilon} \frac{\sinh \left(\frac{\pi}{\beta} (x_3^+ - x_0^+) \right) \sinh \left(\frac{\pi}{\beta} (x_0^+ - x_2^+) \right)}{\sinh \left(\frac{\pi}{\beta} (x_3^+ - x_2^+) \right)} \right]$$

for the region : $x_0^+ < x_3^+$ and $x_3^- < x_0^- < x_5^-$.

(A.17)

Similar results hold for the other regions. By combining the above results and $S_\beta[\bar{C}]$, we get the final expression for the entire region in the universe B .

Until now, we have focused on the CFT entanglement entropy of the two disjoint intervals. However, we easily can extend the above analysis to the single interval case by removing either region \bar{C}_1 or \bar{C}_2 and following the similar procedure.

References

- [1] A. Almheiri, R. Mahajan, J. Maldacena and Y. Zhao, *The Page curve of Hawking radiation from semiclassical geometry*, *JHEP* **03** (2020) 149 [[1908.10996](#)].
- [2] A. Almheiri, N. Engelhardt, D. Marolf and H. Maxfield, *The entropy of bulk quantum fields and the entanglement wedge of an evaporating black hole*, *JHEP* **12** (2019) 063 [[1905.08762](#)].
- [3] G. Penington, *Entanglement Wedge Reconstruction and the Information Paradox*, *JHEP* **09** (2020) 002 [[1905.08255](#)].
- [4] G. Penington, S. H. Shenker, D. Stanford and Z. Yang, *Replica wormholes and the black hole interior*, [1911.11977](#).
- [5] A. Almheiri, T. Hartman, J. Maldacena, E. Shaghoulian and A. Tajdini, *Replica Wormholes and the Entropy of Hawking Radiation*, *JHEP* **05** (2020) 013 [[1911.12333](#)].
- [6] S. Ryu and T. Takayanagi, *Holographic derivation of entanglement entropy from AdS/CFT*, *Phys. Rev. Lett.* **96** (2006) 181602 [[hep-th/0603001](#)].
- [7] S. Ryu and T. Takayanagi, *Aspects of Holographic Entanglement Entropy*, *JHEP* **08** (2006) 045 [[hep-th/0605073](#)].
- [8] V. E. Hubeny, M. Rangamani and T. Takayanagi, *A Covariant holographic entanglement entropy proposal*, *JHEP* **07** (2007) 062 [[0705.0016](#)].
- [9] T. Faulkner, A. Lewkowycz and J. Maldacena, *Quantum corrections to holographic entanglement entropy*, *JHEP* **11** (2013) 074 [[1307.2892](#)].
- [10] N. Engelhardt and A. C. Wall, *Quantum Extremal Surfaces: Holographic Entanglement Entropy beyond the Classical Regime*, *JHEP* **01** (2015) 073 [[1408.3203](#)].

- [11] D. N. Page, *Information in black hole radiation*, *Phys. Rev. Lett.* **71** (1993) 3743 [[hep-th/9306083](#)].
- [12] D. N. Page, *Time Dependence of Hawking Radiation Entropy*, *JCAP* **09** (2013) 028 [[1301.4995](#)].
- [13] A. Almheiri, T. Hartman, J. Maldacena, E. Shaghoulian and A. Tajdini, *The entropy of Hawking radiation*, [2006.06872](#).
- [14] V. Balasubramanian, A. Kar, O. Parrikar, G. Sárosi and T. Ugajin, *Geometric secret sharing in a model of Hawking radiation*, *JHEP* **01** (2021) 177 [[2003.05448](#)].
- [15] M. Rozali, J. Sully, M. Van Raamsdonk, C. Waddell and D. Wakeham, *Information radiation in BCFT models of black holes*, *JHEP* **05** (2020) 004 [[1910.12836](#)].
- [16] H. Z. Chen, R. C. Myers, D. Neuenfeld, I. A. Reyes and J. Sandor, *Quantum Extremal Islands Made Easy, Part I: Entanglement on the Brane*, *JHEP* **10** (2020) 166 [[2006.04851](#)].
- [17] H. Z. Chen, R. C. Myers, D. Neuenfeld, I. A. Reyes and J. Sandor, *Quantum Extremal Islands Made Easy, Part II: Black Holes on the Brane*, *JHEP* **12** (2020) 025 [[2010.00018](#)].
- [18] I. Akal, Y. Kusuki, N. Shiba, T. Takayanagi and Z. Wei, *Entanglement Entropy in a Holographic Moving Mirror and the Page Curve*, *Phys. Rev. Lett.* **126** (2021) 061604 [[2011.12005](#)].
- [19] H. Geng, A. Karch, C. Perez-Pardavila, S. Raju, L. Randall, M. Riojas et al., *Information Transfer with a Gravitating Bath*, [2012.04671](#).
- [20] K. Kawabata, T. Nishioka, Y. Okuyama and K. Watanabe, *Probing Hawking radiation through capacity of entanglement*, [2102.02425](#).
- [21] H. Geng, Y. Nomura and H.-Y. Sun, *An Information Paradox and Its Resolution in de Sitter Holography*, [2103.07477](#).
- [22] S. Falls and S. F. Ross, *Islands and mixed states in closed universes*, [2103.14364](#).
- [23] L. Anderson, O. Parrikar and R. M. Soni, *Islands with Gravitating Baths*, [2103.14746](#).
- [24] T. Li, J. Chu and Y. Zhou, *Reflected Entropy for an Evaporating Black Hole*, *JHEP* **11** (2020) 155 [[2006.10846](#)].
- [25] I. Akal, *Universality, intertwiners and black hole information*, [2010.12565](#).
- [26] F. Deng, J. Chu and Y. Zhou, *Defect extremal surface as the holographic counterpart of Island formula*, *JHEP* **03** (2021) 008 [[2012.07612](#)].
- [27] A. Bhattacharya, A. Bhattacharyya, P. Nandy and A. K. Patra, *Islands and complexity of eternal black hole and radiation subsystems for a doubly holographic model*, [2103.15852](#).
- [28] V. Balasubramanian, A. Kar and T. Ugajin, *Entanglement between two disjoint universes*, *JHEP* **02** (2021) 136 [[2008.05274](#)].
- [29] V. Balasubramanian, A. Kar and T. Ugajin, *Islands in de Sitter space*, *JHEP* **02** (2021) 072 [[2008.05275](#)].

- [30] T. Hartman, Y. Jiang and E. Shaghoulian, *Islands in cosmology*, *JHEP* **11** (2020) 111 [[2008.01022](#)].
- [31] Y. Chen, V. Gorbenko and J. Maldacena, *Bra-ket wormholes in gravitationally prepared states*, *JHEP* **02** (2021) 009 [[2007.16091](#)].
- [32] W. Sybesma, *Pure de Sitter space and the island moving back in time*, [2008.07994](#).
- [33] C. G. Callan, Jr., S. B. Giddings, J. A. Harvey and A. Strominger, *Evanescent black holes*, *Phys. Rev. D* **45** (1992) R1005 [[hep-th/9111056](#)].
- [34] T. M. Fiola, J. Preskill, A. Strominger and S. P. Trivedi, *Black hole thermodynamics and information loss in two-dimensions*, *Phys. Rev. D* **50** (1994) 3987 [[hep-th/9403137](#)].
- [35] J. G. Russo, L. Susskind and L. Thorlacius, *Black hole evaporation in (1+1)-dimensions*, *Phys. Lett. B* **292** (1992) 13 [[hep-th/9201074](#)].
- [36] K. Hashimoto, N. Iizuka and Y. Matsuo, *Islands in Schwarzschild black holes*, *JHEP* **06** (2020) 085 [[2004.05863](#)].
- [37] T. Hartman, E. Shaghoulian and A. Strominger, *Islands in Asymptotically Flat 2D Gravity*, *JHEP* **07** (2020) 022 [[2004.13857](#)].
- [38] T. Anegawa and N. Iizuka, *Notes on islands in asymptotically flat 2d dilaton black holes*, *JHEP* **07** (2020) 036 [[2004.01601](#)].
- [39] C. Krishnan, V. Patil and J. Pereira, *Page Curve and the Information Paradox in Flat Space*, [2005.02993](#).
- [40] F. F. Gautason, L. Schneiderbauer, W. Sybesma and L. Thorlacius, *Page Curve for an Evaporating Black Hole*, *JHEP* **05** (2020) 091 [[2004.00598](#)].
- [41] Y. Matsuo, *Islands and stretched horizon*, [2011.08814](#).
- [42] X. Wang, R. Li and J. Wang, *Islands and Page curves of Reissner-Nordström black holes*, *JHEP* **04** (2021) 103 [[2101.06867](#)].
- [43] X. Wang, R. Li and J. Wang, *Islands and Page curves for a family of exactly solvable evaporating black holes*, [2104.00224](#).
- [44] H. Geng, S. Lüster, R. K. Mishra and D. Wakeham, *Holographic BCFTs and Communicating Black Holes*, [2104.07039](#).
- [45] V. Balasubramanian, A. Kar and T. Ugajin, *Entanglement between two gravitating universes*, [2104.13383](#).
- [46] J. Maldacena and L. Susskind, *Cool horizons for entangled black holes*, *Fortsch. Phys.* **61** (2013) 781 [[1306.0533](#)].
- [47] P. Calabrese and J. Cardy, *Entanglement and correlation functions following a local quench: a conformal field theory approach*, *J. Stat. Mech.* **0710** (2007) P10004 [[0708.3750](#)].
- [48] P. Caputa, M. Nozaki and T. Takayanagi, *Entanglement of local operators in large- N conformal field theories*, *PTEP* **2014** (2014) 093B06 [[1405.5946](#)].

- [49] M. Nozaki, T. Numasawa and T. Takayanagi, *Holographic Local Quenches and Entanglement Density*, *JHEP* **05** (2013) 080 [[1302.5703](#)].
- [50] C. T. Asplund, A. Bernamonti, F. Galli and T. Hartman, *Holographic Entanglement Entropy from 2d CFT: Heavy States and Local Quenches*, *JHEP* **02** (2015) 171 [[1410.1392](#)].
- [51] P. Caputa, J. Simón, A. Štikonas, T. Takayanagi and K. Watanabe, *Scrambling time from local perturbations of the eternal BTZ black hole*, *JHEP* **08** (2015) 011 [[1503.08161](#)].
- [52] T. Ugajin, *Two dimensional quantum quenches and holography*, [1311.2562](#).
- [53] C. T. Asplund and A. Bernamonti, *Mutual information after a local quench in conformal field theory*, *Phys. Rev. D* **89** (2014) 066015 [[1311.4173](#)].
- [54] M. Nozaki, T. Numasawa and T. Takayanagi, *Quantum Entanglement of Local Operators in Conformal Field Theories*, *Phys. Rev. Lett.* **112** (2014) 111602 [[1401.0539](#)].
- [55] M. Nozaki, *Notes on Quantum Entanglement of Local Operators*, *JHEP* **10** (2014) 147 [[1405.5875](#)].
- [56] P. Caputa, J. Simón, A. Štikonas and T. Takayanagi, *Quantum Entanglement of Localized Excited States at Finite Temperature*, *JHEP* **01** (2015) 102 [[1410.2287](#)].
- [57] J. R. David, S. Khetrpal and S. P. Kumar, *Universal corrections to entanglement entropy of local quantum quenches*, *JHEP* **08** (2016) 127 [[1605.05987](#)].
- [58] T. J. Hollowood and S. P. Kumar, *Islands and Page Curves for Evaporating Black Holes in JT Gravity*, *JHEP* **08** (2020) 094 [[2004.14944](#)].
- [59] K. Goto, T. Hartman and A. Tajdini, *Replica wormholes for an evaporating 2D black hole*, [2011.09043](#).
- [60] H. Z. Chen, Z. Fisher, J. Hernandez, R. C. Myers and S.-M. Ruan, *Information Flow in Black Hole Evaporation*, *JHEP* **03** (2020) 152 [[1911.03402](#)].
- [61] H. Z. Chen, Z. Fisher, J. Hernandez, R. C. Myers and S.-M. Ruan, *Evaporating Black Holes Coupled to a Thermal Bath*, *JHEP* **01** (2021) 065 [[2007.11658](#)].
- [62] T. J. Hollowood, S. Prem Kumar and A. Legramandi, *Hawking radiation correlations of evaporating black holes in JT gravity*, *J. Phys. A* **53** (2020) 475401 [[2007.04877](#)].
- [63] T. Hartman, S. Jain and S. Kundu, *Causality Constraints in Conformal Field Theory*, *JHEP* **05** (2016) 099 [[1509.00014](#)].
- [64] Y. Chen, *Pulling Out the Island with Modular Flow*, *JHEP* **03** (2020) 033 [[1912.02210](#)].
- [65] A. L. Fitzpatrick, J. Kaplan and M. T. Walters, *Universality of Long-Distance AdS Physics from the CFT Bootstrap*, *JHEP* **08** (2014) 145 [[1403.6829](#)].